Exp 594

UPPER LIMIT FOR ν_μ OSCILLATION INTO ν_τ IN A DICHROMATIC BEAM

by

Juan Bofill Abadias

B. S. Massachusetts Institute of Technology

SUBMITTED IN PARTIAL FULFILLMENT

OF THE REQUIREMENTS FOR THE

DEGREE OF DOCTOR OF PHILOSOPHY

at the

MASSACHUSETTS INSTITUTE OF TECHNOLOGY

Signature of Author . . . . . .

Physics Department

june 19, 1984

Certified by . . . . . .

Thesis Supervisor

Accepted by . . . . . .

Chairman, Physics Graduate

Committee

To my family and to the memory of my grand father.

ABSTRACT

Limits on the mass squared difference of neutrino mass eigenstates $\delta^2 = |m_1^2 - m_2^2|$, have been determined in a fine grained calorimeter exposed to the dichromatic beam at Fermilab. The fine grained calorimeter is located at a distance of 1.3 Km from the neutrino source making it suitable for oscillations studies. The interaction of a $\nu_\tau(\overline{\nu}_\tau)$ with nucleons resulting in $\tau^{\pm}$ production is considered. In this interaction, it is assumed that a $\nu_\tau(\overline{\nu}_\tau)$ interacts quasi-elastically and that the produced $\tau^{\pm}$ decays into the two leptonic channels $\mu^{\pm} + \nu_\tau(\overline{\nu}_\tau) + \nu_\mu(\overline{\nu}_\mu)$ or $e^{\pm} + \nu_\tau(\overline{\nu}_\tau) + \nu_e(\overline{\nu}_e)$. The capability of this calorimeter to distinguish electron from hadron showers and its capability to measure muon energy is exploited to determine the limits on δ^2.

CONTENTS

ABSTRACT

I. THE OSCILLATION AMONG NEUTRINO SPECIES.

II. EXPERIMENTAL SETUP.

III. QUASI ELASTIC INTERACTIONS.

IV. DESCRIPTION OF THE DETECTOR.

THE CALORIMETER

MUON SPECTROMETER

V. MUON CHANNEL ANALYSIS.

VI. ELECTRON CHANNEL ANALYSIS.

VII. COMPARISON WITH OTHER EXPERIMENTS.

VIII. CONCLUSIONS.

IX. ACKNOWLEDGEMENTS.

X. REFERENCES.

FIGURE CAPTIONS

1) Overall view of FERMILAB.

2) Narrow band beam setup during the 1982 run.

3) E vs. R plot for the π band only from Monte Carlo beam simulation.

4) E vs. R plot for the K band only from Monte Carlo beam simulation.

5) E vs. R plot for $K_{\mu 3}$ three body decays from Monte Carlo.

6) E vs. R plot for K_{e3} three body decays from Monte Carlo.

6.a) Kinematics defining diagram.

7) Muon momentum in the lab from τ decay.

8) Muon momentum in the C.M. from τ decay.

9) Detector

10) Module of the flash chamber calorimeter.

11) Flash chamber readout scheme.

12) Schematics of the proportional plane amplifiers.

13) Hadron angle resolution.

14) Electron angle resolution.

15) Toroid cross section.

16) Aluminum module used in the proportional planes.

17) Resistive charge network.

18) Δ distributions for eigth series resistors.

19) Muon momentum resolutions.

20) E vs. R plot during the -165 Gev and +165 Gev exposures for quasi-

elastic events.

21) y_{vis} distribution for data vs. quasi Monte Carlo events.

22) y_{vis} distribution for data vs. tau Monte Carlo events.

23) Reconstructed $R_{90\%}$ distribution.

24) E vs. R plot for wide band background shape.

25) δ^2 vs. $\sin^2 2\theta$ plot from the -165 GeV quasi elastic muon events.

26) δ^2 vs. $\sin^2 2\theta$ plot from the +165 GeV quasi elastic muon events.

27) Diagram defining quantities used in the calculation of ρ and w.

28) w vs. ρ plot for electron showers.

29) w vs. ρ plot for hadron showers.

30) Muon multiplicity along the X_{view} for real events vs. fake events.

31) Δl distribution.

32) Δw distribution.

33) $\Delta \rho$ distribution.

34) $nbox$ distribution for neutral vs. charged current events.

35) ρ distribution for neutral vs. charged current events.

36) l distribution for neutral vs. charged current events.

37) w distribution for neutral vs. charged current events.

38) Illustration on the calculation of the upper limit.

39) δ^2 vs. $\sin^2 2\theta$ upper limit plot for the -165 GeV run from the electron channel analysis.

40) δ^2 vs. $\sin^2 2\theta$ upper limit plot for the +165 GeV run from the electron

channel analysis.

41) δ^2 vs. $\sin^2 2\theta$ upper limit plot for the +200 GeV run from the electron channel analysis.

42) δ^2 vs. $sin^2 2\theta$ upper limit plot for the +250 GeV from the electron channel analysis.

I. THE OSCILLATION AMONG NEUTRINO SPECIES

The possibility of massive neutrinos is an open question both in terms of experiment and theory. For massive neutrinos, it is possible that they mix to some level. Such mixing Hypotheses date back to 1957[1]. At present, the Weinberg-Salam[2] theory has succesfully described many of the weak-interaction properties and in particular, it has passed a crucial test in predicting the mass of the W and Z with the measured θ_W.[3,37,42] on the other hand, the theory has no predictive power for lepton (or quark) masses and there are no hints regarding the possibility of mixing among members of the lepton sector in analogy with the Cabbibo mixing of the quark sector. In general a mixing matrix for the lepton sector can be introduced. For the three neutrino species case, the mixing is accomplished by adding a term to the Weinberg -Salam Lagrangian of the form:

$$\mathcal{L}^{lept}_{mass} \alpha (\bar{e}_L \bar{\mu}_L \bar{\tau}_L) m \begin{pmatrix} e_R \\ \mu_R \\ \tau_R \end{pmatrix} \qquad I.1$$

Where e, μ, τ stand for Fermi fields and L, R are the right and left handed components, and m is some mixing matrix. The physical neutrinos will then turn out to be linear combinations of the Dirac massive fields:

$$(\nu_e \nu_\mu \nu_\tau) = U \begin{pmatrix} \nu_1 \\ \nu_2 \\ \nu_3 \end{pmatrix} \qquad I.2$$

The U is a matrix similar to the Kobayashi-Maskawa matrix. In this experiment, only the mixing between ν_μ and ν_τ neutrinos is considered. In this case the mixing matrix is just:

$$\begin{pmatrix} \nu_\mu \\ \nu_\tau \end{pmatrix} = \begin{pmatrix} \cos\theta & \sin\theta \\ -\sin\theta & \cos\theta \end{pmatrix} \begin{pmatrix} \nu_1 \\ \nu_2 \end{pmatrix} \qquad I.3$$

In the standard treatment[4,5,38], it is supposed that we have a beam of neutrinos all having a common, fixed momentum p_ν. It is also usually assumed that all the masses m_n are much smaller than p_ν. In this beam, the mass eigenstates ν_n will have energy $E_n(p_\nu) = \sqrt{p_\nu^2 + m_n^2} \approx p_\nu + (\frac{m_n^2}{2p_\nu})$. If a neutrino in this beam is born with definite flavor $f = \mu, \tau$ at time $t = 0$, then at time $t = 0$ its wave function will be:

$$|\nu_f(x, t = 0) >= \sum_n U_{fn} \nu_n e^{ip_\nu x} \qquad I.4$$

After a time t this will evolve into:

$$|\nu_f(x, t) >= \sum_n U_{fn} \nu_n e^{ip_\nu x} e^{-iE_i t} \qquad I.5$$

Since this neutrino is highly relativistic, if it was born at $x = 0$, then at time t it will be at $x \approx t$. At that point the above function is:

$$|\nu_f(t, t) > \approx \sum_n U_{fn} \nu_n e^{-i(\frac{m_n^2}{2p_\nu})t} \qquad I.6$$

If we start with a pure flavor f, say μ, the probability P of finding the neutrino to have a flavor $f = \tau$ at a distance $x = L$ from its source is given by:

$$P(\nu_\mu \to \nu_\tau) = |< \nu_\tau(L, t = L)|\nu_\mu(0, 0) >|^2 \qquad I.7$$

Where:

$$|\nu_\mu(0,0)>=\cos\theta|\nu_1>+\sin\theta|\nu_2> \qquad I.8$$

$$|\nu_\tau(0,0)>=0 \qquad I.9$$

$$|\nu_\tau(L,t=L)>=-\sin\theta|\nu_1>e^{-iE_1L}+\cos\theta|\nu_2>e^{-iE_2L} \qquad I.10$$

Taking the product $<\nu_\tau(L,t=L)|\nu_\mu(0,0)>$ and then its magnitude squared gives:

$$P(\nu_\mu\rightarrow\nu_\tau)=\sin^2 2\theta\sin^2\frac{(E_1-E_2)L}{2} \qquad I.11$$

Substituting for E_1 and E_2 gives:

$$P(\nu_\mu\rightarrow\nu_\tau)=\sin^2 2\theta\sin^2 1.27\frac{\delta^2 L}{E_\nu} \qquad I.12$$

where $\delta^2=|m_1^2-m_2^2|$ in eV^2, L in Km and E_ν in GeV. The purpose of this experiment will be to search for ν_τ events in order to set upper limits on the mass squared difference as a function of the mixing angle θ.

II. *EXPERIMENTAL SETUP*

In this chapter, a short description of this experiment is given with a description of the interactions searched for. The experiment uses a proton beam from the 400 GeV proton synchrotron of the Fermi National Accelerator Laboratory in Batavia, Illinois. The accelerator, a proton synchrotron, is schematically shown in figure 1.

The protons are produced by ionizing hydrogen gas. The protons are accelerated to $\approx$750 KeV by a Cockcroft-Walton, accelerated then to 200 MeV by a linac and then to a few GeV by a booster synchroton. After the booster synchrotron, the protons are injected into the main ring where energies of up to 400 GeV were achieved.

The protons are extracted from the main ring and distributed to several laboratories so that more than one type of experiment could be carried out simultaneously. In particular, the proton beam was sent to the Neutrino Laboratory where neutrinos are produced and distributed to different fixed target neutrino experiments. This experiment is located at the end of the neutrino line at Lab C.

To produce neutrinos, the 400 Gev proton beam is steered towards a BeO target where during collision with the target nucleons, $\pi^{\pm}$ and $K^{\pm}$ mesons are predominantly produced. The $\pi^{\pm}$ and $K^{\pm}$ each have major two body

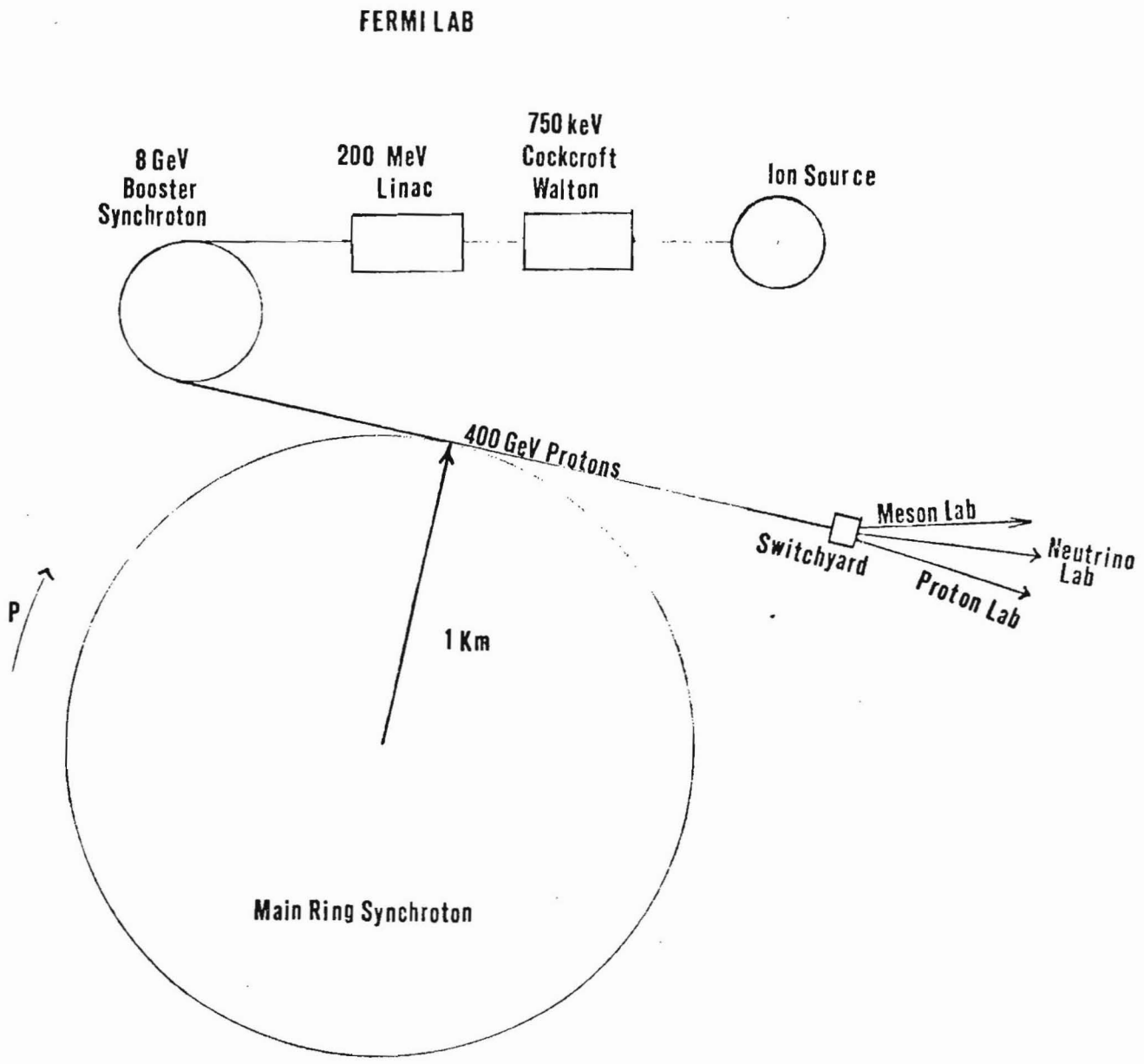
FERMI LAB
8 GeV
Booster
Synchroton
200 MeV
Linac
750 keV
Cockcroft
Walton
Ion Source
400 GeV Protons
Meson Lab
Switchyard
Neutrino
Lab
Proton Lab
P
1 Km
Main Ring Synchroton

Figure 1.

decay modes $\mu^{\pm} + \nu_\mu(\overline{\nu}_\mu)$; the branching ratios B.R.are $\approx$100%and $\approx$ 65% respectively[16]. For a given π or K energy the two body decay kinematics is particulary simple; the neutrino energy spectra is flat ranging from:

$$0 < \frac{E_\nu}{E_{\pi,K}} < 1 - \frac{m_\mu^2}{M_{\pi,K}^2} \qquad II.1$$

In addition, because of the two body kinematics, there is a one to one relationship between energy and angle of neutrino for a given parent π or K momentum, making possible an energy selected beam. There will also be three body decays of $K \rightarrow \pi + \mu + \nu_\mu$ and $K \rightarrow e + \pi + \nu_e$. These two decay modes give rise to neutrinos without the energy angle correlation mentioned above which are an unwanted background flux for most experiments. The B.R. for these decays are small ($\approx$ 5%) and thus contamination of ν_μ and ν_e from three body decays is small. With the beam configuration for this experiment, the ratio of 3 body ν_μ and ν_e with respect to the π-decay ν_μ neutrinos is .47%and .88%respectively. In addition to $\pi^{\pm}$ and $K^{\pm}$, other heavier charmed mesons like $D^{\pm}$ and $F^{\pm}$ can be produced. Because of their large mass, these mesons are expected to decay "promptly" into neutrinos. The lifetimes for these heavy mesons are $\tau \approx 10^{-12}$sec compared to the $\pi^{\pm}$ and $K^{\pm}$ lifetimes $\tau \approx 2.6 \times 10^{-8}$sec and $\tau \approx 1.24 \times 10^{-8}$sec respectively. Since this experiment is fundamentally a search for ν_τ interactions, the prompt ν_τ would also be detected in principle in this study. In what follows, a crude estimate is given on the number of ν_τ events that look like charge

current events in the detector based on experimental results from beam dump studies[6,7,8,9].

At the time of writing, these experiments are still subject to interpretation[15] and their results are subject to change; so caution is in order. In the CHARM prompt neutrino experiment, a ratio of $\frac{\nu_e+\overline{\nu}_e}{\nu_\mu+\overline{\nu}_\mu} = .48\pm.12$ prompt neutrinos is reported[10]. These authors also quote a prompt $\nu_\mu + \overline{\nu}_\mu$ rate of 0.176 $\frac{events}{Ton 10^{17} P.O.T.}$ ($P.O.T.$ is a standard term that stands for protons on target). In this experiment, we have 1.5×10^{18} $P.O.T.$, 130 tons of fiducial volume. We assume that all the $\nu_e + \overline{\nu}_e$ come from $D^{\pm} \rightarrow e^{\pm} + \nu_e(\overline{\nu}_e) + X$ with a measured B.R. $= .2$[11,12]. Assume that the ratio of F production to D production is 0.1. (This is a conservative estimate and the measured hadronic F production will likely be smaller[13]) Assuming that the mass of the $\nu_\tau < 250$ MeV, then the decay chain $F \rightarrow \tau + \nu_\tau$ and $\tau \rightarrow \nu_\tau + X$ is the primary ν_τ source. This sequence of events gives as much as a factor of 2 in the ν_τ yield. The B.R. for $F \rightarrow \nu_\tau + \tau$ is estimated to be .03.[14] Since we are concerned with events that look like ν_μ charged current events in the detector, we must include the B.R.=.18 (measured[16,17]) for $\tau \rightarrow \mu + \nu_\mu + \nu_\tau$. Finally putting a threshold factor of $\approx \frac{1}{2}$ for the τ production yields:

$$\frac{0.176}{10^{17}} \times .48 \times \frac{1}{.2} \times 0.1 \times 2 \times 0.03 \times 0.18 \times \frac{1}{2}$$

$$\times 1.5 \times 10^{18} \times 130 = .44 \quad events$$

The software efficiency to detect these events will further reduce the chance

to see them at all. Thus it is assumed that the ν_τ prompt production can be ignored in the rest of this experiment.

In order to produce a Dichromatic Beam (also known as a Narrow Band Beam) the produced hadrons (ie. the π and K) are momentum selected before they decay.(See figure 2). The selection is accomplished by requiring that the initial proton beam, point sufficiently away from the neutrino detectors. In this way, only the momentum selected hadron beam is steered towards the detector. After the momentum selection, the hadron beam is allowed to decay in the decay tunnel. Following the decay tunnel, a massive shield absorbs the hadrons or muons left at the end of the decay pipe. The neutrino energy at the detector is given as a function of the parent momentum and decay angle by:

$$E_\nu = \gamma P^* \frac{2}{1 + \gamma^2 \sin^2 \theta_L} \qquad II.2$$

where P^* is the CM momentum of the decay neutrino, γ is the Lorentz Factor for decaying meson $\gamma = \frac{E_{\pi,K}}{M_{\pi,K}}$ and θ_L is the laboratory decay angle.

The above neutrino energy can be writen in terms of the quantities defined in figure 2 :

$$E_\nu = E_{\pi,K}(1 - \frac{m^2}{M^2_{\pi,K}})[\frac{1}{1 + (\frac{E_{\pi,K}}{M})^2 \sin^2 \theta_L}] \qquad II.3$$

and the decay angle can be written as:

$$\sin \theta_L = \frac{\frac{r}{L + xL_D}}{\sqrt{1 + (\frac{r}{L + xL_D})^2}} \qquad II.4$$

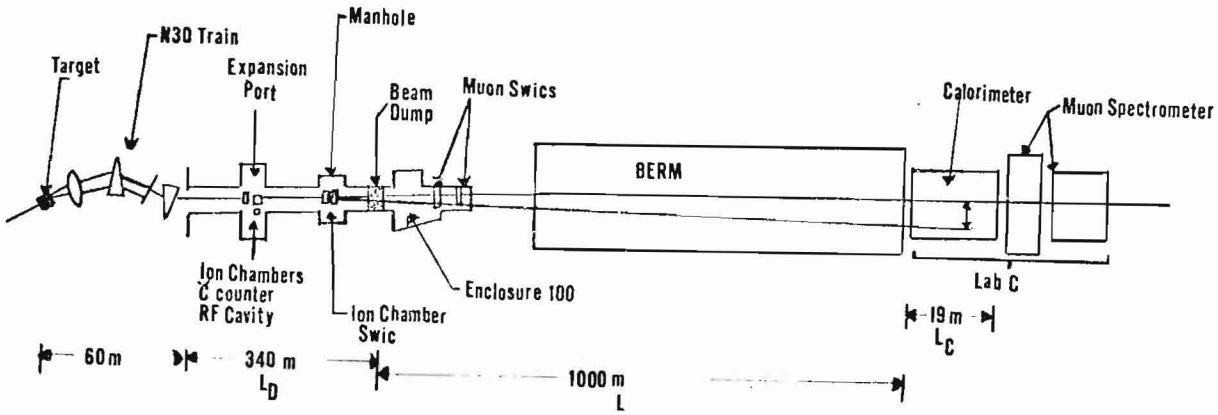

figure 2

where L is the distance from the end of the decay tunnel to the detector, L_D is the decay pipe length, r is the radius from the beam center at the detector, x is related to an exponentially distributed variable defining the decay point of the parent particles, $E_{\pi,K}$ is the energy of π, K parent particles, $M_{\pi,K}$ parent particle mass, m is the decay lepton mass. This gives rise to a Lorentz-Shaped curve in a E vs r plot at the detector as shown in figures 3 and 4. The neutrino energy spread at a given r is mainly due to the momentum spread and angular divergence of the hadron beam after momentum selection and the decay positions of the produced hadrons. The two bands correspond to the π and K decays. The events between the bands are in part due to the three body decays of these mesons. Figures 5 and 6 show the E vs r plot for

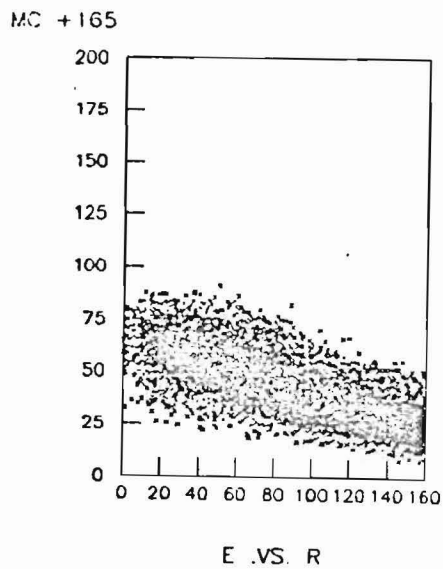

figure 3

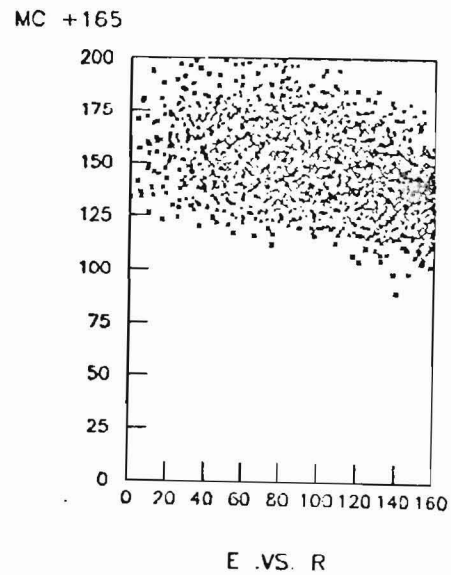

figure 4

these decays.

The Dichromatic Beam, is instrumented with ion chambers, an R.F. cavity and a Cherenkov counter to monitor the secondary flux and composition. Pressure curves are taken with the Cerenkov counter to measure the $K - \pi$ band ratio while the R.F.cavity and the ion chambers measured the flux of secondary particles. The primary proton flux was also measured with a beam toroid. These measurements are used to compute neutrino cross sections.

Having produced ν_μ neutrinos in quantities, the hypothesis that a ν_μ oscillates into a ν_τ neutrino can be studied in this detector with the assumption that the ν_τ interacts quasi elastically. This will be explained shortly but

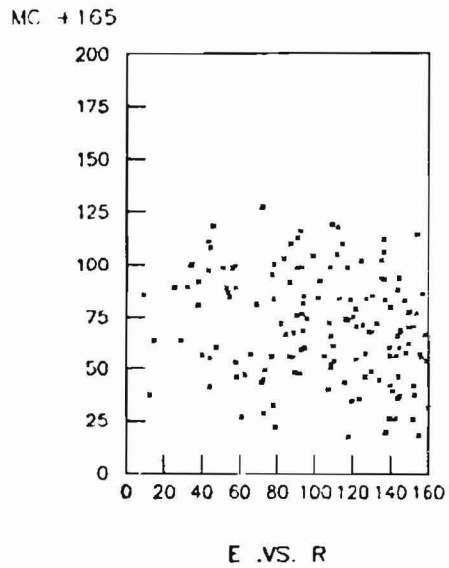

figure 5

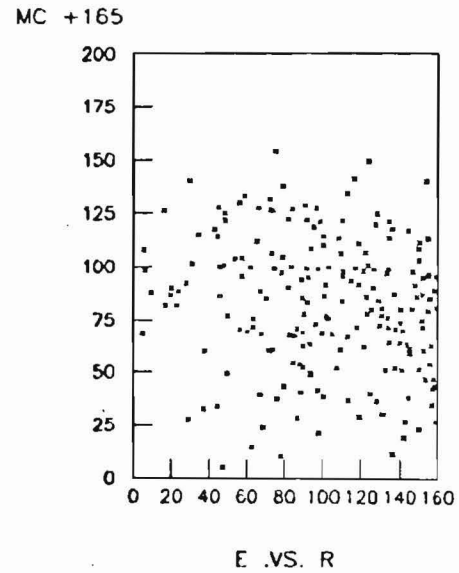

figure 6

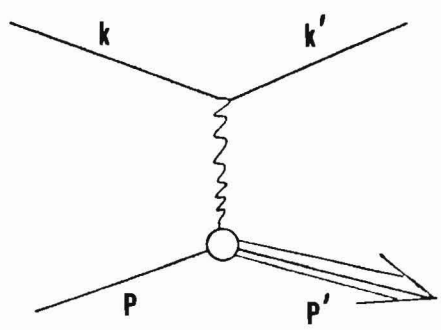

figure 6.a

before doing so, we will define the kinematics pertinent to this experiment.

Referring to figure 6.a, k is the four vector for the incoming lepton, k' is the four vector of the outgoing lepton, P is the four vector of the initial nucleon state and P' is the four vector for the outgoing excited state. Thus by four vector conservation:

$$k + P = k' + P' \qquad II.5$$

Scaling variables are defined by:

$$x = \frac{Q^2}{2M\nu} \quad \nu = \frac{p.q}{M} \quad y = \frac{\nu}{E_\nu}$$

Where in terms of the lepton angle θ in the lab frame:

$$-Q^2 = q^2 = (k - k')^2 = m^2 - 4E_\nu E'_l \sin^2 \frac{\theta}{2} \qquad II.6$$

$$\nu = (E_\nu - E'_l) = (E_h - M) \qquad II.7$$

$$W^2 = P'^2 = (q + P)^2 = m^2 - 2MEy(x - 1) \qquad II.8$$

The x and y variables are kinematically bounded by:

$$x_{min} = \frac{m_\tau^2}{2M(E_\nu - m)} \qquad x_{max} = 1 \qquad II.9$$

$$y_{min}^{max} = \frac{(1 - \delta_\tau(\frac{1}{x} + 2\delta_n)) \pm ((1 - \frac{\delta_\tau}{x})^2 - \frac{m^2}{E^2})^{.5}}{2(\delta_n x + 1)} \qquad II.10$$

where $\delta_i = \frac{m_i}{2ME_\nu}$, M is the nucleon mass, m is the lepton mass, E_ν is the incoming neutrino energy, E'_l is the outgoing lepton l' energy and E_h is the excited hadron energy.

III. *QUASI ELASTIC INTERACTION*

In this interaction a $\nu_\tau + n \rightarrow p + \tau^-$ or $\overline{\nu}_\tau + p \rightarrow n + \tau^+$. The kinematics of this interaction follows from relations II.5 throught II.8 by setting $W^2 = M^2 - 2MEy(x-1) = M^2$. It then follows that x=1 and the entire event is described by two independent variables namely y and E_ν.

The calculation of the cross section for this interaction involves the calculation of the hadronic vertex described by an amplitude of the form:

$$W_{\mu\nu} = \sum_{spin} \sum_{I} < N|J_\nu^+|I >< I|J_\nu|N > \delta(q + P - P') \qquad III.0$$

This can be evaluated in terms of six measurable form factors. The details can be found in references 18 and 19. Here the result is quoted:

$$\frac{d\sigma^{\nu,\overline{\nu}}}{dq^2} = \frac{M^2 G^2 \cos^2\theta_c}{8\pi E_\nu^2}(A(q^2) + B(q^2)\frac{(s-u)}{M^2} + C(q^2)\frac{(s-u)^2}{M^4}) \qquad III.1$$

Where $s = (k+P)^2$, $u = (k-P')^2$ are the Mandelstam variables; $A(q^2)$, $B(q^2)$ and $C(q^2)$ are linear combinations of the form factors. The various Hypotheses about the weak interaction, restricts the form factors as follows:

1) T invariance $\rightarrow$ All form factors are real.

2) TC invariance $\rightarrow F^3_{V,A} = 0$

3) CVC $\rightarrow F^3_V = 0$

From experimental evidence on muon capture, F_p has been determined to be small. We will assume $F_p = 0$. Under these assumptions the $A(q^2)$, $B(q^2)$

and $C(q^2)$ can be written as:

$$A(q^2) = \frac{(m^2 - q^2)}{4M^2}((4 - \frac{q^2}{M^2})|F_A|^2 - (4 + \frac{q^2}{M^2})|F_V^1|^2 - \frac{q^2}{M^2}|\xi F_V^2|^2(1 + \frac{q^2}{4M^2})$$

$$-\frac{4q^2}{m^2}F_V^1 \xi F_V^2 - \frac{m^2}{M^2}(|F_V^1 + \xi F_V^2|^2 + (\frac{q^2}{M^2} - 4)|F_V^3|^2)) \qquad III.2$$

The $B(q^2)$ term is given by:

$$B(q^2) = -\frac{q^2}{M^2}F_A(F_V^1 + \xi F_V^2) - \frac{m^2}{M^2}(F_V^1 + \frac{q^2}{4M^2}\xi F_V^2)F_V^3 \qquad III.3$$

And the $C(q^2)$ term is:

$$C(q^2) = \frac{1}{4}(|F_A|^2 + |F_V{}'|^2 - \frac{q^2}{M^2}|\frac{\xi F_V^2}{2}|^2) \qquad III.4$$

$$F_A(q^2) = -1.23(1 - \frac{q^2}{M_A^2})^{-2} \qquad III.5$$

$$F'_V(q^2) = (1 - \frac{q^2}{4M^2})^{-1}(G_E^V(q^2) - \frac{q^2}{4M^2}G_M^V(q^2)) \qquad III.6$$

$$\xi F_V^2(q^2) = (1 - \frac{q^2}{4M^2})^{-1}(G_M^V(q^2) - G_E^V(q^2)) \qquad III.7$$

The G's are described experimentally to within 10%by[18]:

$$G_E^V(q^2) = \frac{1}{(1 - \frac{q^2}{.71})^2}, \quad G_M^V(q^2) = \frac{1 + \xi}{(1 - \frac{q^2}{.71})^2} \qquad III.8$$

$\xi = \mu_p - \mu_n = 3.71$ is the difference between the magnetic moment of the proton μ_p and the magnetic moment of the neutron μ_n. That leaves the parameter M_A to be found from experiment. The experimental results on

this parameter are consistent with a value of M_A =1.0 GeV[20]. This is the quasi elastic cross section for ν_μ and $\overline{\nu}_\mu$. From now on, it will be assumed to be a correct description for ν_τ interactions. With this cross section, the distribution of the produced τ lepton can be predicted up to its polarization. But the polarization of the τ at these energies is of order $P_L(\tau^{\pm}) \approx^{\pm} 1 + O(\frac{m_\tau^2}{E_l'})$ with E_l'= energy of the outgoing τ. Therefore, the τ is produced with strong longitudinal polarization.

The produced τ has a short lifetime[21] $\tau_\tau = 2.3 \times 10^{-13}$ sec. The mean free path for such a short lifetime is of the order of $470\mu m$ at 10 GeV. This means that in this calorimeter (described later), a direct observation of the τ is not possible. However, the decay products of the τ will have properties that will distinguish such events from other processes. The distribution, in its rest frame, of the final state charged lepton l from the decay of the $\tau \rightarrow l + \nu_l + \nu_\tau$ is given by:[22]

$$dW = K\frac{d\Omega}{4\pi}\left(\frac{1+h(x)}{1+4n\frac{m_\mu}{m_\tau}}\left(12(1-x) + \frac{4}{3}\rho(8x-6) + 24\frac{m_\mu}{m_\tau}\frac{(1-x)}{x}\eta\right) + \right.$$

$$\left.\xi\cos\theta\left(4(1-x) + \frac{4}{3}\delta(8x-6) + \frac{\alpha}{2\pi}\frac{g(x)}{x^2}\right)\right)x^2dx \qquad III.9$$

Where $x = \frac{\overline{P}_\mu}{\overline{P}_{max}}$ and $h(x)$ and $g(x)$ are radiative corrections. The best experimental values for the Michel parameters[23,24]are consistent with $\rho = \frac{3}{4}$, $\eta = 0$, inserting these values, the above expression becomes simply:

$$\frac{dW}{d\Omega} = K(1-\xi\cos\theta)\left(\frac{1-2x}{3-2x}\right))x^2 2(3-2x)dx \qquad III.10$$

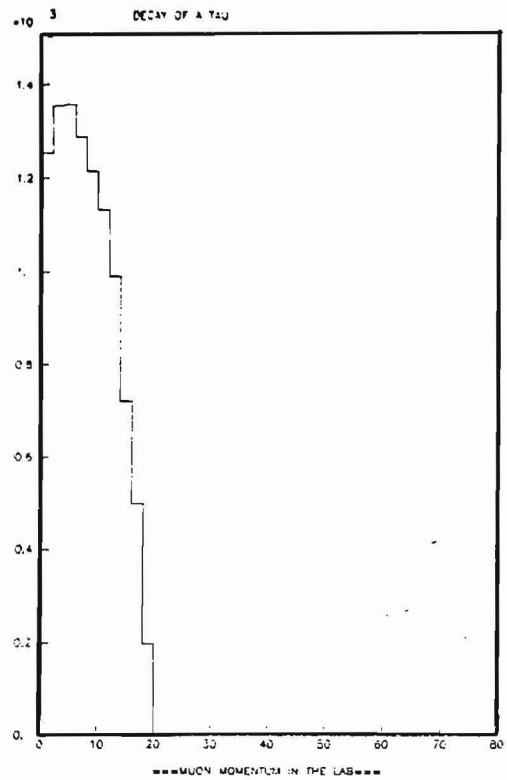

figure 7

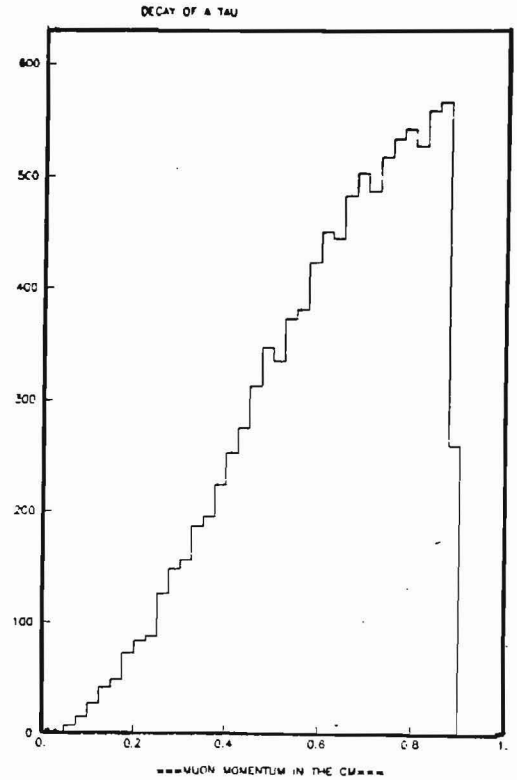

figure 8

With $\xi = -1$ for τ^- and $\xi = +1$ for τ^+. This means that the e^+, μ^+ prefer to be emitted along the direction of the τ^+ spin and e^-, μ^- prefer to be emitted opposite to the direction of the τ^- spin[39,44]. The momentum distribution of the final state muon is shown in figure 7 for the ideal case of a τ beam in the lab at a fixed momentum of 20 GeV. Figure 8 shows the momentum distribution of the final state muon in the C.M. system.

The fact that there is a substantial amount of energy carried out by the two neutrinos in the τ decay will be the key feature in trying to identify ν_τ interactions in this experiment. The experimental details will be described in the sections MUON ANALISIS and ELECTRON ANALISIS.

IV. *DESCRIPTION OF THE DETECTOR*

THE CALORIMETER

In order to study neutrino-induced interactions, and in particular neutral current interactions, it is desirable to have a massive detector capable of measuring the energy and angle of the reaction products. To measure these quantities, we have constructed a fine grained calorimeter backed up with a muon spectrometer. [25,45,47] See figure 9. The calorimeter is based on polypropylene flash chambers and proportional tube chambers. These chambers provide a very high degree of segmentation. The calorimeter is 19 metres long and has a 3.6×3.6 mts^2 cross section with a mass of $\approx$ 340 metric tons. The flash chambers are used for pattern recognition to determine the type of interaction as well as to determine the average angle and energy flow of the reaction products. The proportional tubes provide the trigger to the flash chambers and they also provide a measurement of the energy flow. There are a total of 608 flash chambers, 37 proportional tubes, 304 target planes of steel shot, 304 target planes of sand and 7 planes of liquid scintillators. The construction of the calorimeter is modular. Each module is made up of four 4" $\times$ 4" wide iron beams with 4 flash chambers mounted on each in the sequence U-X-Y-X, where U-X-Y stand for flash chambers with cells running at $100^0 - 0^0 - 80^0$ degrees relative to the horizontal plane

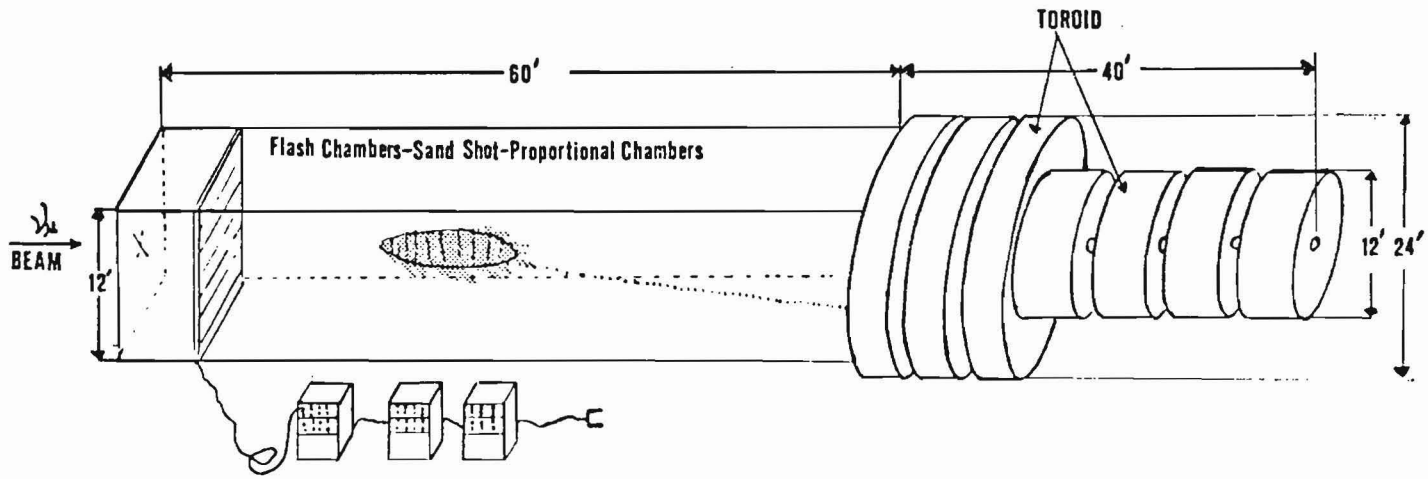
TOROID
60′
40′
Flash Chambers-Sand Shot-Proportional Chambers
BEAM
12′
12′
24′

figure 9

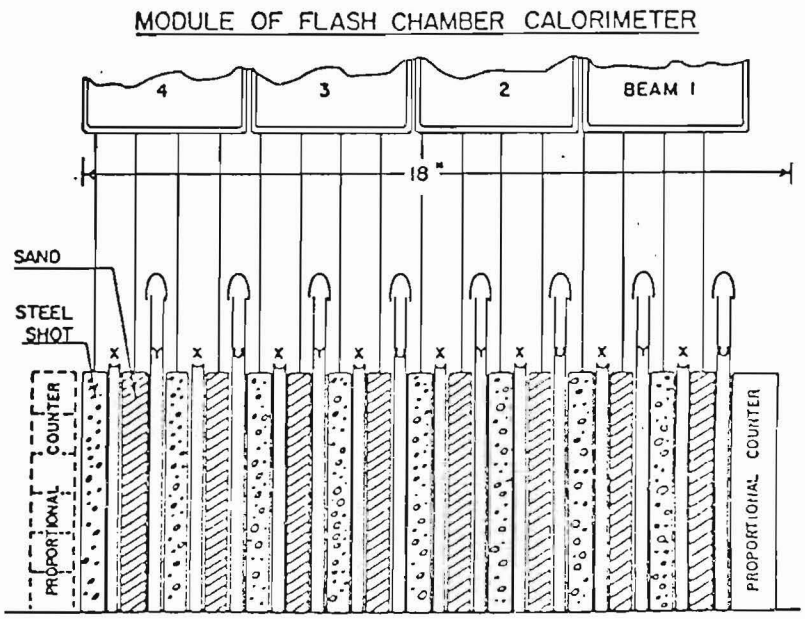

figure 10

respectively. See figure 9. Between the flash chambers, steel shot planes and sand planes are alternated. To complete the modules, one proportional tube plane is placed upstream of the assembly just described. The next module has the same structure except that the proportional plane has wires running perpendicular to that in the previous module. This construction with the choice of sand and steel shot is a good practical solution to get good angular resolutions, energy resolutions and neutrino event rate simultaneously. With this geometry, the flash chambers sample every 22%of a radiation length(radlen=13 cm)and 3.1%of an absortion length (abslen=97 cm) and the proportional tubes sample every 340%of a radiation length and 49%of an absortion length[25].

The flash chambers are constructed from polypropylene extrusions with 5. mm$\times$5.8 mm rectangular cells. A mixture of 90%-10%Ne-He gas flows througth the cells. After a charged particle traverses a flash chamber, if a high voltage (9 kvolts) is applied to it, a plasma discharge will occur in the traversed cell. This plasma propagates down the cell towards the edge of the chamber. At one end, copper strips are laid along the flash chamber cells and connected to ground. See figure 11. These copper strips form a set of capacitors to ground whose capacitance changes during the plasma discharge. This change in capacitance induces a current pulse along the copper strip which in turn is picked up by a magnetostrictive wand. The pulses from the magnetotrisctive wand are clocked. The clock frequency is set to 2 clock counts per cell with a novel scheme that avoids synchronization problems and ambiguities caused by variations in cell separation[25].

The digital information from the cells is stored on tape with a PDP-11 via CAMAC crates. This information is used to determine the shower energy as well as the direction of energy flow. These two quantities are of crucial importance in trying to study neutral current induced interactions.

The proportional tubes in the detector are made up of 12' long aluminum extrusions with eight 1"$\times$1" cells in each extrusion. Eighteen of these extrussions are stacked edge to edge to make a proportional tube plane. Each cell is strung with a 50μm gold plated tungsten anode wire. A gas mixture of 90%argon and 10%methane flows through the cells. On each plane j

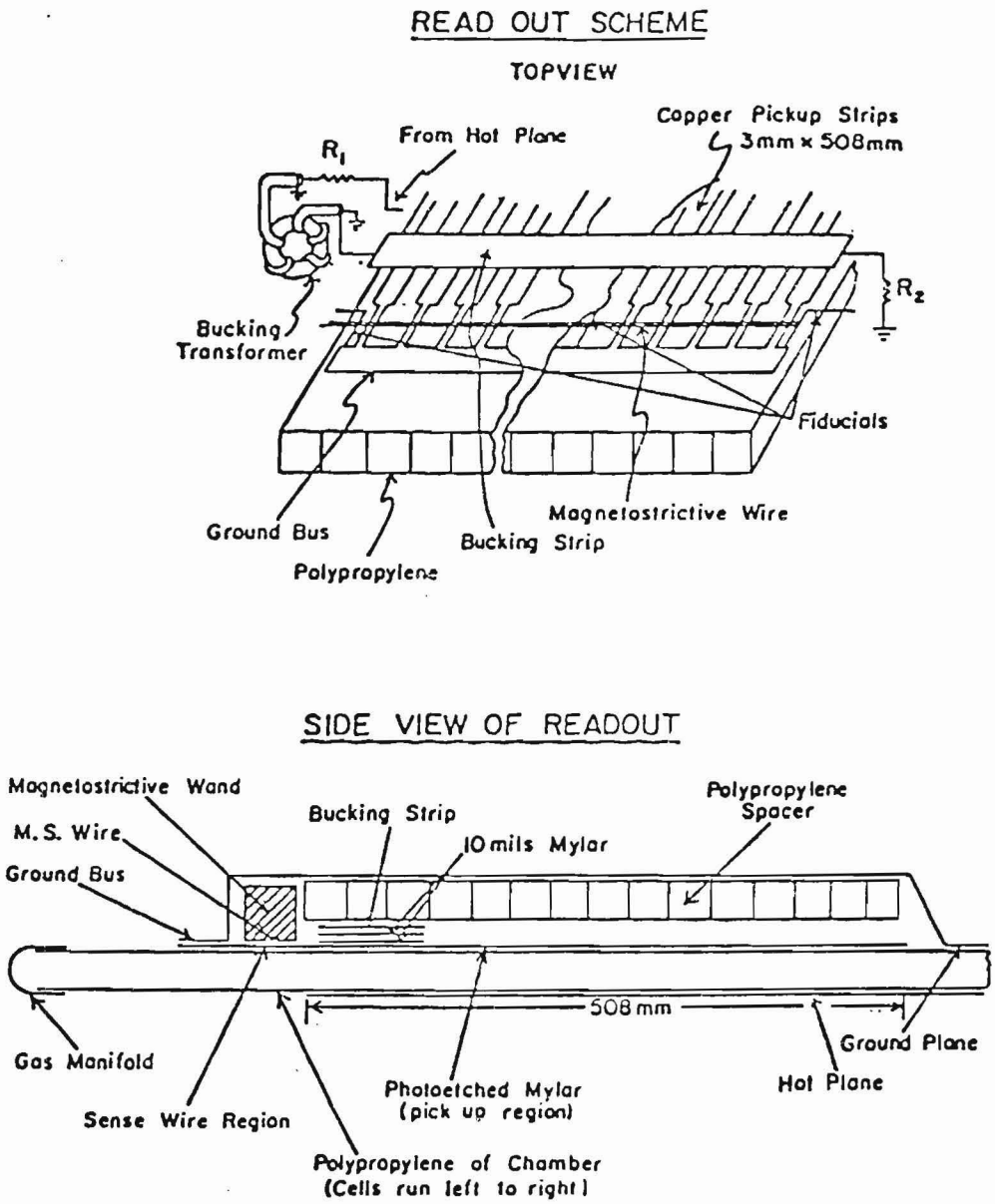
READ OUT SCHEME
TOPVIEW
Copper Pickup Strips
3mm x 508mm
From Hot Plane
R_1
R_2
Bucking Transformer
Fiducials
Ground Bus
Polypropylene
Bucking Strip
Magnetostrictive Wire
SIDE VIEW OF READOUT
Magnetostrictive Wand
M.S. Wire
Ground Bus
Bucking Strip
10 mils Mylar
Polypropylene Spacer
508 mm
Gas Manifold
Sense Wire Region
Photoetched Mylar (pick up region)
Polypropylene of Chamber (Cells run left to right)
Ground Plane
Hot Plane

figure 11

there is a total of 36 charge amplifiers, i=1...36, each of them connected to 4 wires. Each of the 36 charge amplifiers provide a fast out analog signal called FO_{ij}. This FO_{ij} is split into two equal components. See figure 12. One of the components is added with the corresponding output of the rest of the 36 amplifiers to make a fast out signal for the whole plane called "sum out"$\equiv \sum_j \equiv \sum_{i=1}^{36} FO_{ji}$. The other component of the FO_{ij} is discriminated within each plane j and it is used in the development of several triggers. A brief description of the proportional tube information follows:

1)Sum out $\sum_j = \sum_{i=1}^{36} FO_{ij}$. This signal is added for all planes into $\sum\sum = \sum_{j=1}^{37}(\sum_j)$. It is a fast trigger and it is a measure of the total energy deposited in the calorimeter.

2)Single (S_i): This signal is a logical "or" of all discriminated FO_{ij} within plane j. The Threshold of each plane for each channel j could be easily changed to suit a specific trigger requirement.

3)Analog Multiplicity AM_j: As the name implies, it is an analog signal whose amplitude is proportional to the number of FO_{ij} $i = 1...36$ channels above discriminator level within plane j.

4)Analog Multiplicity Multiplicity N>i>j: It is a multiplicity condition on the AM_j condition for all j=1...37 planes in the calorimeter.

5)M : Analog signal made by the requirement that the $\sum_j$ on two or more planes be above a fixed threshold.

The high voltage applied to the wires in the calorimeter planes is 1650

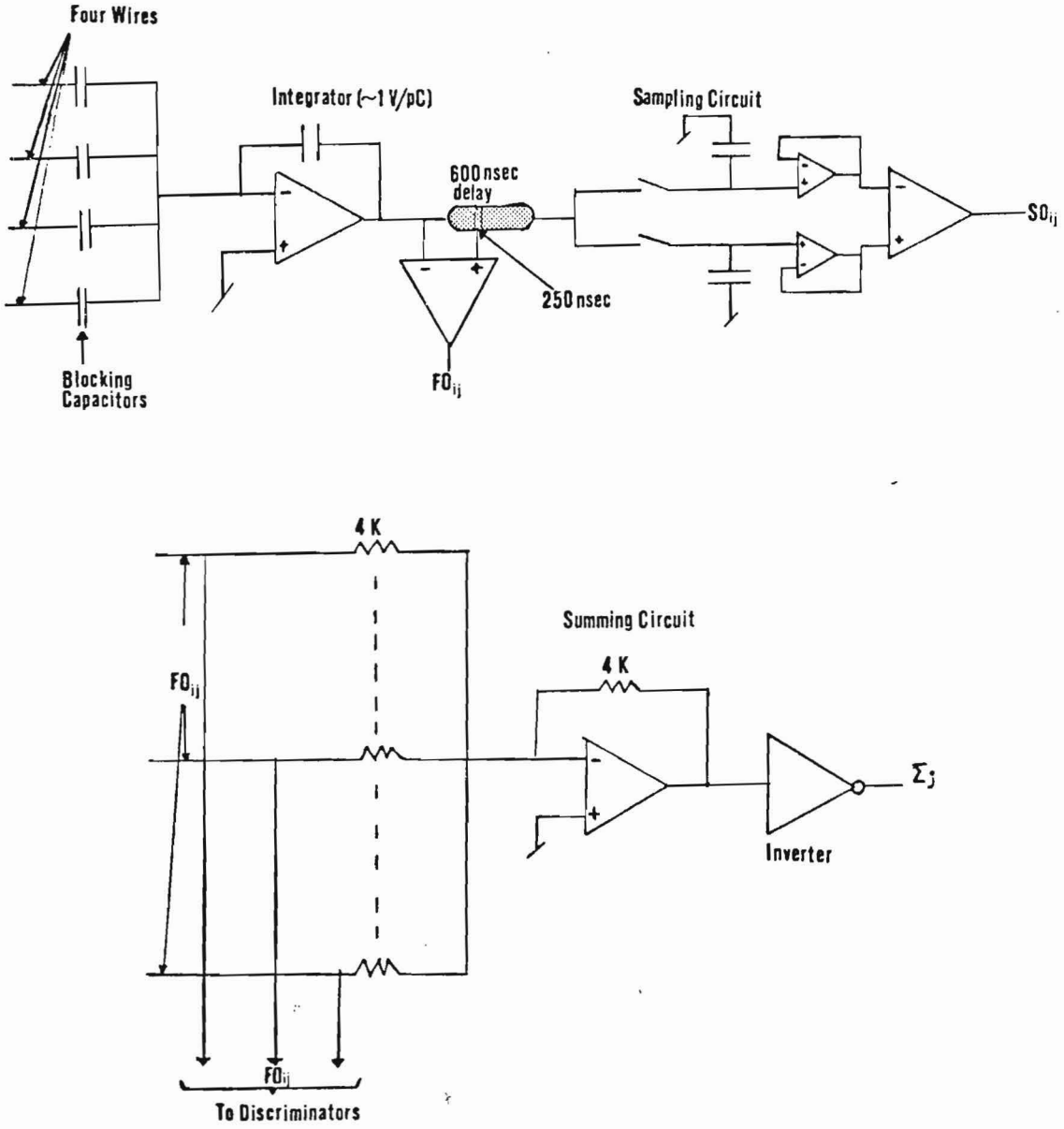
Four Wires
Integrator (~1 V/pC)
Sampling Circuit
600 nsec
delay
250 nsec
SO_{ij}
Blocking
Capacitors
FO_{ij}
4 K
Summing Circuit
4 K
FO_{ij}
Σ_j
Inverter
FO_{ij}
To Discriminators

figure 12

Volts corresponding to a gas gain of 3000. With this setup, the 230 ion pairs produced by a minimum ionizing particle give rise to an average FO_{ij} pulse height of $\approx$ 90 mV into a 50Ω termination. The above proportional tube information is used to develop different types of triggers. The specific trigger used in the Dichromatic Beam in connection with this experiment, will be discussed later in the "MUON CHANNEL ANALYSIS" and "ELECTRON CHANNEL ANALYSIS" sections.

Besides the fast out information described so far, the signal from the input integrating amplifier is delayed and sampled by a track and hold circuit (this signal is called "slow out" SO_{ji}. The charge stored in the track and hold capacitors is read out by a scanner. This scanner is connected to a CAMAC crate that transmits the digitized information from the scan to a PDP-11 where the information is stored on tapes. The proportional tube gains were calibrated with Cd^{109} sources placed on each cell of the proportional planes. Calibration events are logged between accelerator spills recording the pulse heights of the Cd_{109} x-ray sources mounted on each proportional tube.

Apart from providing the trigger, the proportional tubes also give information on the total energy deposited in the calorimeter. This information is added to the information from the flash chamber hits in the final calculation of the shower energy.

CALORIMETER RESPONSE: The calorimeter response is studied with test calibration beams of known energy and incoming angle during the

1982 run. Three test beams are used: a hadron beam, an electron beam and a muon beam. The determination of the calorimeter response (resolutions) follows:

ANGLE RESOLUTIONS: The calorimeter is calibrated with a test hadron beam of known energies in the range of 20 to 100 GeV. The hadron calibration beam impinged on the detector under a fixed angle. The results of the survey of the beam[26] result in:

X view $\theta_x = 0$

y_0 view $\theta_{y_0} = 68.9 \pm .2$ mrad

Where the y_0 view is measured in the U and Y flash chamber views and is related by :

$$\tan\theta_{y_0} = \frac{1}{2\cos\theta}(\tan\theta_U + \tan\theta_Y) \qquad IV.1$$

Where θ is the angle between the flash chamber cells and the x axis ($\theta = 10^0$).

The angle of the shower is measured from the calorimeter flash chamber hits. Two algorithms have been developed to find the shower angle: Hadflow and Shang. Hadflow fits the shower axis by a minimum χ^2 method which treats all three flash chamber views simultaneously with the primary vertex position fixed. The calculation of the χ^2 depends on weigths determined in each iteration from the lateral distribution of hits. Shang determines the angle of a shower by means of an angular histogram. The shower hits N are binned into angular cells θ_i emanating from the fixed vertex. For each

cell θ_i, the number of hits n_i is counted. The angle in a given flash chamber view is calculated from:

$$\theta_{view} = \sum_{i=1}^{N} \frac{n_i \theta_i}{n_i} \qquad IV.2$$

These two angle finders have been shown to give the same results. The angle resolutions have been found as follows: for each event, the angle in the U, X, Y views and the y_0 view is determined and entered in a histogram. The resulting distribution is fitted by a gaussian. The sigma of the distribution is used as the resolution at a particular energy in the sample. The process is repeated as a function of energy. The obtained $\sigma_\theta(E_h)$ are fitted as a function of energy. The result is:

$$\sigma_{\theta_x}(E_h) = (7.3 + \frac{1008}{E_h}) \qquad IV.3$$

$$\sigma_{\theta_{y_0}}(E_h) = (11.0 + \frac{1064}{E_h}) \qquad IV.4$$

Where θ_x and θ_y are the projected polar angles in mrad in the x and y flash chamber views respectively and E_h is the shower energy in GeV. Figure 13 shows the data points and the fit to the combined polar angle θ_p.

The same algorithm is used to determine the electron angle resolutions. Calibration electrons in the range 5 to 35 GeV are taken. The resolutions have been found in the same manner as in the hadron case. The result is for electron showers:

$$\sigma(\theta_p) = (6.92 + \frac{91.9}{E_e}) \qquad IV.5$$

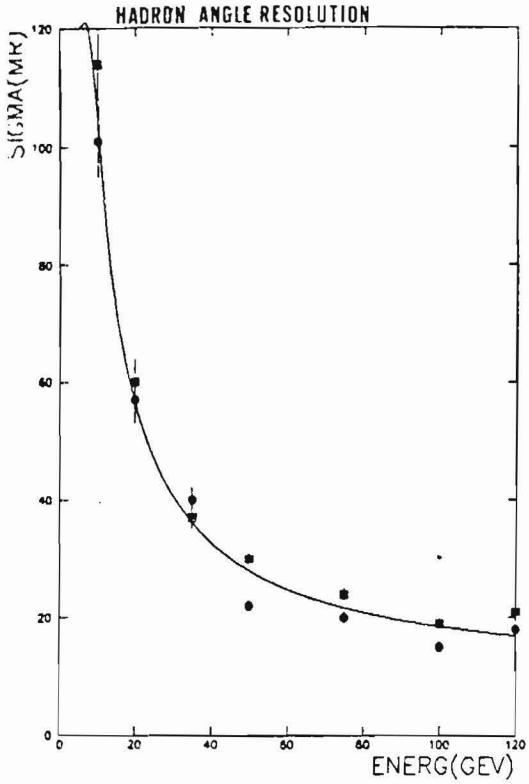

figure 13

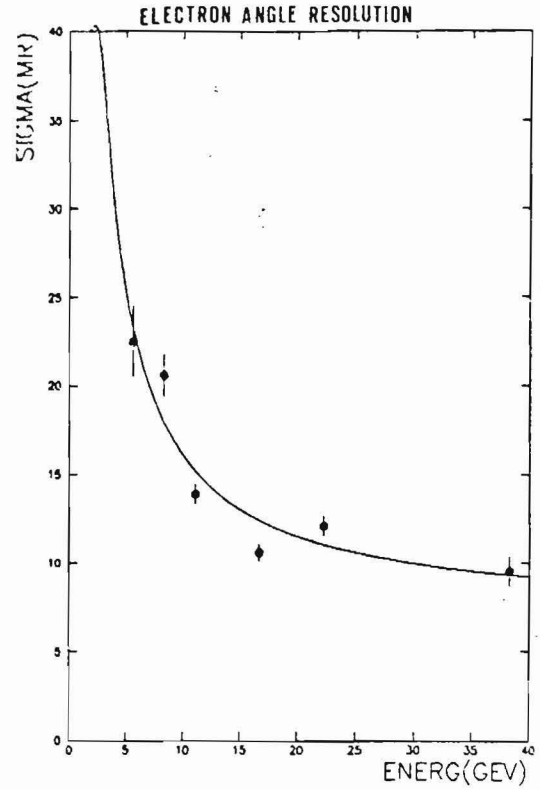

figure 14

where θ_p is the shower polar angle in mrad and E_e is the electron energy in GeV. See figure 14.

ENERGY RESPONSE: The test data are used both to calibrate and measure the energy resolution of the calorimeter. The energy of a shower can be measured by counting the total number of flash chamber hits. The relation between total number of hit cells and the energy of the shower is nonlinear because of the saturation of flash chamber cells in the shower core. Thus, the energy resolutions will depend on the nonlinear behaviour of the calorimeter and fluctuations in the total visible energy. Such effects are empirically corrected for in the algoritm used to measure the shower energy. To find the energy resolution as a function of energy, a histogram is filled with

the calculated energies for each event at a fixed test energy. The resulting distribution is fitted with a gaussian and the sigma is used as the energy resolution. The resulting sigmas $\sigma(E_h)$ are fitted as a function of energy. The result is:

$$\sigma(E_h) = (0.052 + \frac{0.519}{\sqrt{E_h}})E_h \qquad IV.6$$

MUON ANGLE RESOLUTION: The muon angle resolution is found from a least squares fit to the flash chamber hits left by a muon track. Calibration muons with known incoming angles are used to determine the resolution. The process is similar to the shower angle resolution determination. The result is:

$$\sigma(\theta_\mu) = (1.59 + \frac{97.1}{P_\mu}) \qquad IV.7$$

where θ_μ is the muon polar angle in mrad and P_μ is the muon momentum in GeV.

MUON SPECTROMETER

The Muon Spectrometer[27] in this detector consists of three 24' and four 12' diameter magnetized iron toroids colocated dowstream of the calorimeter as shown in figure 9. The direction of the average magnetic field in these toroids is shown in figure 15. The field magnitude has been measured as a function of radial distance r. A fit to the data, in agreement with calculated field values,[] is given for the 24' toroids by:

$$eB(r,z) = .004122 + \frac{0.1998}{D} \qquad IV.8$$

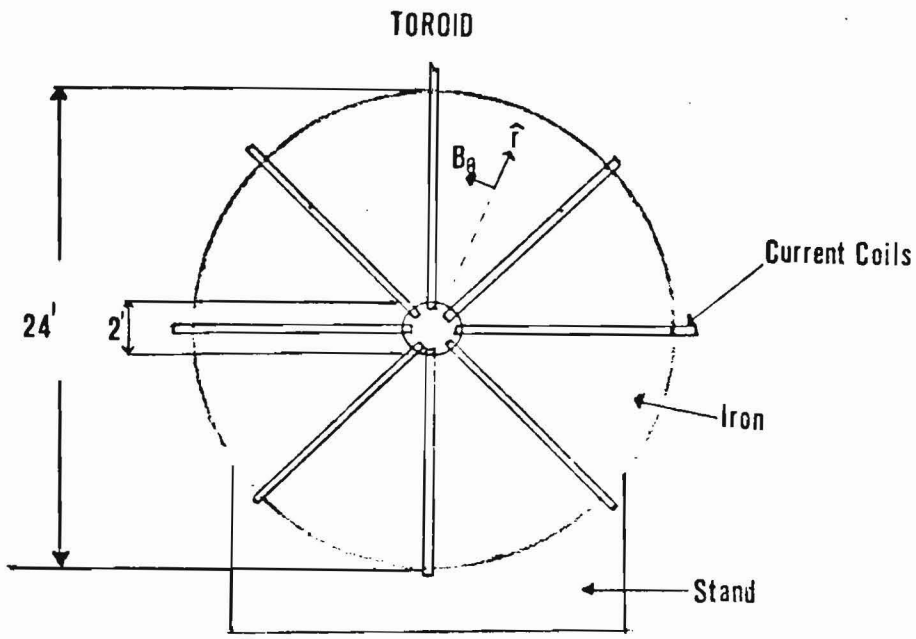

figure 15

$$D = (r + 77.2) \quad cm \quad with \quad 30.5cm \leq r \leq 366cm \qquad IV.9$$

For the 12' toroids, the fields are parametrized by:

$$eB(r,z) = 0.1998 + \frac{2.083}{D} \qquad IV.10$$

$$D = (r - 41.6)r + 1871 \quad with \quad 15.2cm \leq r \leq 183cm \qquad IV.11$$

Where the units are such that with $e = .3 \times 10^{-3} \frac{Gev}{KGcm}$ and r in cm, B(r,z) will be in KG.

The gaps between the toroids are instrumented with proportional chambers. Each gap is instrumented with two double layer chambers with half cell offsets between these two layers, providing two measurements along the horizontal direction and two measurements along the vertical direction. A total of 3456 wires are instrumented.

Each proportional chamber is made up of a stack of double layered aluminum extrusions placed edge to edge. Each extrusion consists of two layers of eight cells with $\frac{1}{2}$ cell displacement as shown in figure 16. The cell cross section is .840" $\times$ .910" rectangle. Three cell lengths are used in the spectrometer: 24',16' and 12'. Each cell is strung with a 50 μm diameter gold-plated tungsten wire. A mixture of 90%Argon 10%Methane flows througth these cells. A d.c. high voltage of 1950 volts is applied between the wire (anode) and the aluminum walls (cathode). With this high voltage, the $\approx$230 ion pairs produced in the gas by a minimum ionizing particle are amplified by a factor of $\approx$ 30000. The electronic configuration of the charge amplifiers is the same as in the calorimeter planes. Figure 12 shows the basic configuration of these amplifiers. The fast out signal FO_{ij} is similar to the calorimeter planes except that its amplitude is $\approx$ 1 Volt into 50Ω.

The $FO_{i,j}$ are added for all 36 channels in plane j into the sum out signal $\sum_j = \sum_{i=1}^{36} FO_{ij}$. This fast out sum $\sum_j$ is used for triggering in conjuction with the calorimeter planes as well as for self triggering the track and hold circuitry of plane j. The 600 nsec delayed pulse is sampled during 300 nsec by the track and hold circuitry. This information will be used to determine which wire was hit in plane j. A qualitative description of how the hit wire is reconstructed follows:(figure 17)

The charge deposited on a wire due to a charged particle passing througth

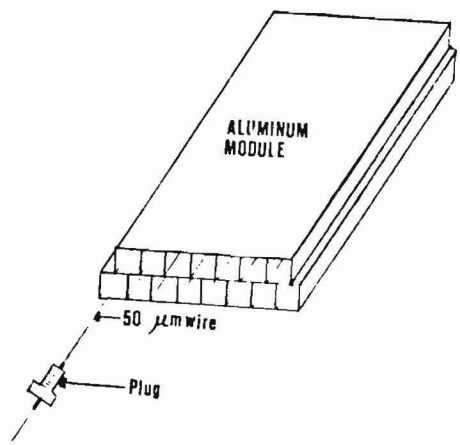

figure 16

the gas, will be split at the resistive lattice junction into dq_j and dq_{j+1} during some time dt small compared to the risetime of the pulse. The current pulses associated with dq_j and dq_{j+1} will have faster or slower risetimes in proportion to the number of resistors that these charges had to travel througth along the resistor lattice. After amplification and delay, this difference in rise time is kept essentially intact. Therefore the amount of sampled charge Q_j and Q_{j+1} will differ in proportion to the number of resistors travelled by the original charge q. Thus by constructing the quantity $\Delta = \frac{Q_{j+1}-Q_j}{Q_{j+1}+Q_j}$, the struck wire can be identified. A range in Δ will correspond to a particular wire being hit within amplifiers j and $j+1$. See figure 18.

The hit wires determine the muon trajectory as it travels down the

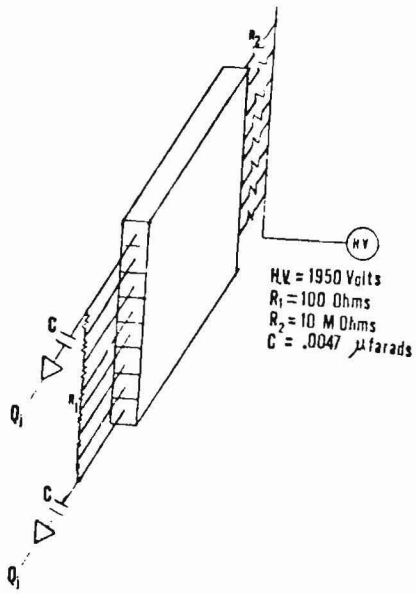

figure 17

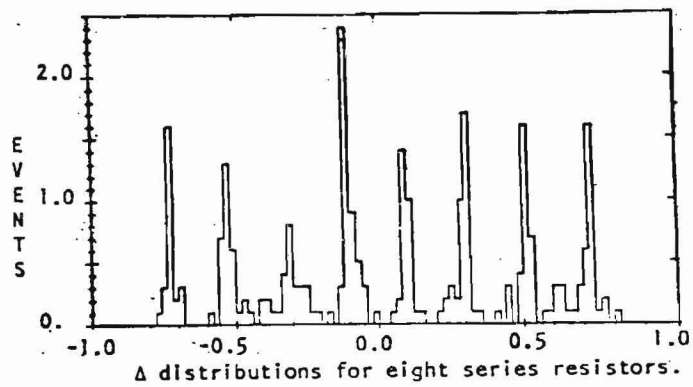

figure 18

spectrometer. The flash chamber hits in the calorimeter and the toroid chamber hits are used to determine the muon momentum. A maximun likelyhood fit to the measured intercepts is found by appoximately linearizing the equaitions of motion and then iterating the fit. Ionization energy loss and multiple coulomb scattering are taken into account.

The spectrometer resolutions are found from calibration muons (ie. form muons with a-priority known momentum). Data was taken at muon momentums in the range 20 GeV to 110 GeV during the 1982 calibration run. For each event an entry is done on a histogram. The R.M.S of the resulting distribution is used to determine the resolution as a function of muon momentum. A fit to the R.M.S. of the distribution gives:

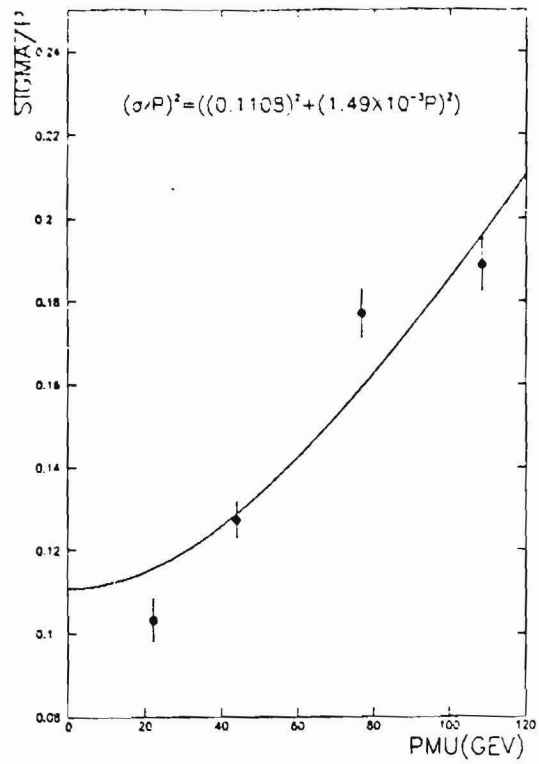

figure 19

$$[\frac{\sigma(P_\mu)}{P_\mu}]^2 = (0.1108)^2 + (1.49 \times 10^{-3} P_\mu)^2 \qquad IV.12$$

where P_μ is the muon momentum in GeV. See figure 19.

V. *MUON CHANNEL – ANALYSIS –*

It is assumed that a $\nu_\tau(\overline{\nu}_\tau)+N \rightarrow \tau^{\pm}+N^*$ where N^* denotes a nucleon or a mildly excited nucleon, and that the produced $\tau^{\pm}$ decays into $\mu^{\pm}+\nu_\mu(\overline{\nu}_\mu)+\nu_\tau(\overline{\nu}_\tau)$. The signature of these events in the calorimeter is a single muon with a small energy deposition around the vertex of the interaction. Only events recorded by use of a special trigger during the +165 GeV and -165 GeV train energy exposures are considered. The trigger required that: 1) a particular muon reached the back chambers of the muon spectrometer and 2) its pulse height from the proportional tubes in the calorimeter correspond to an energy deposition less than $\approx$ 10 GeV (it is relevant here to point out that a muon deposits on the average $\approx$5 GeV traversing the calorimeter). The electronic efficiency of this trigger is found to be 86% from the muon calibration data.

The events are found with pattern recognition programs analysing the hit patterns left in the flash chambers by an event. In this case, a search is done for a muon track leaving the end of the calorimeter. A sequence of least squares fits are done on the muon hits within adjustable roads. At each fit, the road is narrowed and centered about the fit coordinates. The process stops with a road of $\pm$10 clock counts, $\approx$5 cm, where the angular resolutions are found to be optimal. The longitudinal vertex coordinate is

found by an upstream search of muon hits inside the ± 10 clock counts road starting from the end of the calorimeter. The search stops when no hits are found. This determines the longitudinal coordinate of the vertex. The transverse coordinate is the least squres fit coordinate at the longitudinal vertex coordinate. The number of flash chamber hits in a $50cm$ radius around the vertex is added. It is required that this number be < 30 hits. The selected events with the above criteria will not be a pure sample of $\nu_\mu + N \rightarrow \mu^- + P$ or $\bar{\nu}_\mu + P \rightarrow N + \mu^+$. This algorithm will also select single particle production events like $\nu_\mu + N \rightarrow \Delta^+ + \mu^-$ and deep inelastic events $\nu_\mu + N \rightarrow \mu^- + X$ with very low $y = \frac{\nu}{E_\nu}$. The relevant measurable quantities describing such events are expected to be similar to quasi-elastic events. Thus, for the purpose of this experiment, the sample of events left should be well described by the Quasi-Elastic cross section.

Once an event has been selected, the muon momentum is fitted using the hits that the muon left in passing throught the proportional planes in the muon spectrometer. Figure 20 shows the $E(R)$ vs. R correlation plot for the selected events during the +165 GeV and -165 GeV run. The π-band is visible in the plot. From the discussion given in the Quasi-elastic section, events with very low energy are potential ν_τ interactions. With this in mind, in order to define the signal region, the quantity $y_{vis} = \frac{\overline{E}_\nu(R) - E_\mu(R)}{\overline{E}_\nu(R)}$ is reconstructed where $\overline{E}_\nu(R)$ is the average neutrino energy at a distance R from the beam center calculated from the Monte Carlo simulation of the

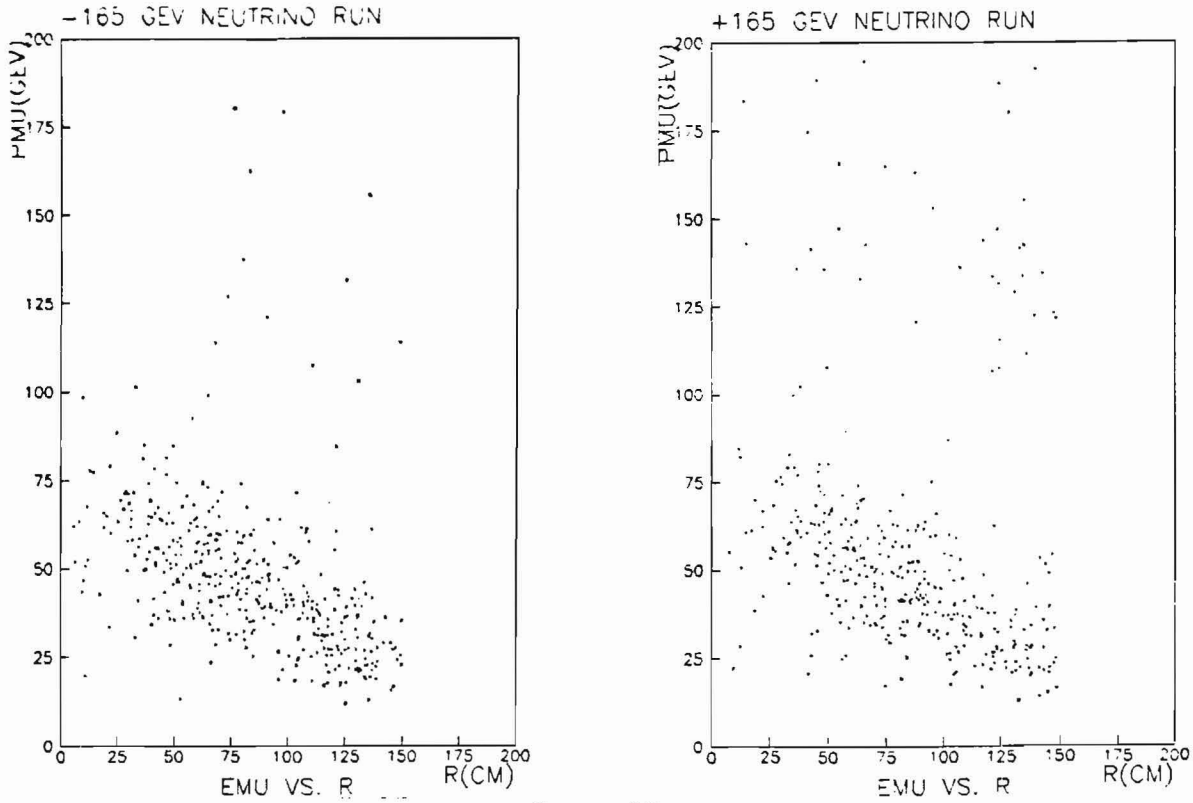

figure 20

Dichromatic Beam and $E_\mu(R)$ is the measured muon momentum. The y_{vis} distribution is reconstructed with data and with Monte Carlo events. The Monte Carlo simulation of quasi-elastic events is done using the Monte Carlo simulation of the beam[46] and the cross section given by equation III.1 for ν_μ or ν_τ quasi-elastic interactions. In the ν_τ quasi-elastic interaction, the produced τ is allowed to decay into $\mu^- + \overline{\nu}_\mu + \nu_\tau$ with the distribution of the outgoing μ dictated by equation III.9. Once the events are generated, they are propagated througth the detector. These events are then analyzed with the same software used to analyze data events. Figure 21 shows the distributions of data and Monte Carlo events.

It apparent that the data agrees quite well with Monte Carlo simulation

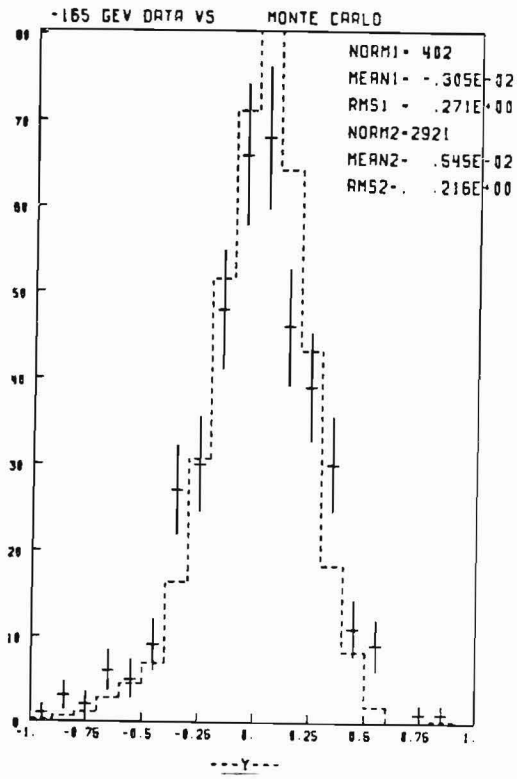

figure 21

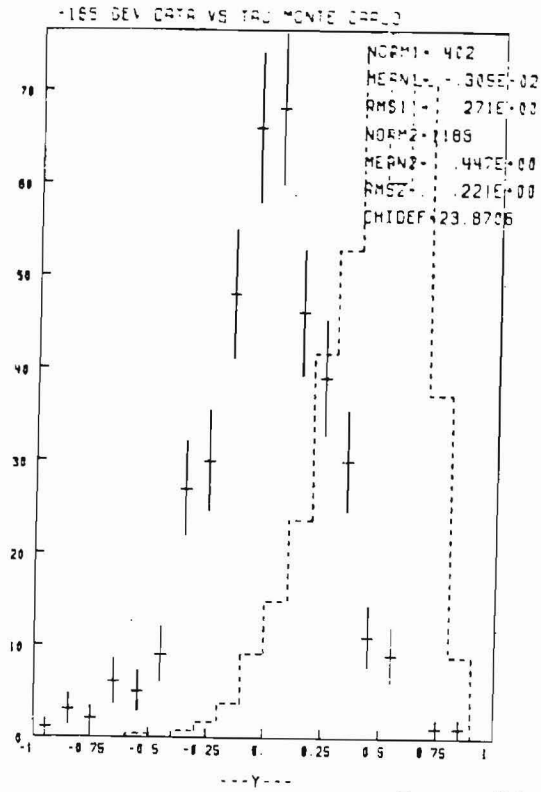

figure 22

under the hypothesis that the Beam is all ν_μ. Figure 22 shows the same y_{vis} distribution vs. Monte Carlo under the ν_τ hypothesis. The distributions are in clear disagreement. As expected, the y_{vis} distribution for ν_τ events is shifted towards positive values. Therefore the region of high y_{vis} will be the region where ν_τ events are more likely to be found. The signal and π-band will be defined as the regions where $y > .6$ and $-1. < y < .6$ respectively.

The signal region is not free of backgrounds. The backgrounds considered in the signal region are:

i) Quasi elastic events with $y > .6$

ii) Wide band background from decays of $\pi - K$ before momentum selection

iii) Inverse muon decay. This decay is due to the interaction of $\nu_\mu + e^- \rightarrow \mu^- \nu_e$. It is a background for the ν_μ exposure only.

In order to estimate the ratio R of ν_τ to ν_μ events that interact in this channel (ie. $\nu_\tau + N \rightarrow N^* + \tau$ with $\tau \rightarrow \mu + \nu_\nu + \nu_\tau$ and $\nu_\mu + N \rightarrow N^* + \nu_\mu$) the following quantities are defined.

$\epsilon^s_{\mu,\tau} = \frac{events\ \ in\ \ signal\ \ region\ \ for\ \ \mu,\tau}{events\ \ in\ \ fiducial\ \ volume\ \ for\ \ \mu,\tau}$ from Monte Carlo

$\epsilon^b_{\mu,\tau} = \frac{events\ \ in\ \ the\ \ \pi-band\ \ region\ \ for\ \ \mu,\tau}{events\ \ in\ \ fiducial\ \ volume\ \ for\ \ \mu,\tau}$ from Monte Carlo

$N_s = number\ \ of\ \ events\ \ found\ \ in\ \ the\ \ signal\ \ region$

$N_b = number\ \ of\ \ events\ \ found\ \ in\ \ the\ \ \pi - band\ \ region$

$N_s = \epsilon^s_\tau N^t_\tau + \epsilon^s_Q N^t_Q = N^t_Q(\epsilon^s_\tau R + \epsilon^s_Q)$

$N_b = \epsilon^b_\tau N^t_\tau + \epsilon^b_Q N^t_Q = N^t_Q(\epsilon^b_\tau R + \epsilon^b_Q)$

$R = \frac{N^t_\tau}{N^t_Q}$

Where N^t_τ and N^t_Q are the number of ν_τ quasi elastic events and ν_μ quasi elastic events after acceptance correction.

No explicit mention of the wide band beam background or the inverse muon background is made in the above expressions but these are both included in the final determination of R. In order to set an upper limit on the estimate of the ratio R, we will reconstruct the distribution $P(R) = \frac{dN}{dR}$ using Poisson distributions for N_s and N_b and the above equations. A family of distributions $\frac{dN}{dR'}$ for particular R' are generated. Then the particular distribution that meets the requirement $.10 = \int_{-\infty}^{R_0} \frac{dN}{dR'} dR'$ is found. The average of this particular distribution is the upper limit on the estimated

R_0, called $R_{90\%}$. Figure 23 shows the distribution we obtained for the $\overline{\nu}$ exposure at -165 GeV train energy.

WIDE BAND BACKGROUND

There is some fraction of the π's and K's produced at the target region that decay before they are momentum selected. The neutrinos from these decays will not show a dichromatic E vs R correlation. See figure 24. These neutrinos show a large energy spread in the E vs R plot and thus they can populate the signal and the $\pi-$band regions as previously defined. It is clear then that these neutrinos can produce some background to the ν_τ signal which must be subtracted to get our best estimate for the τ signal. To estimate this background, an iron plug was placed in the beam just before the momentum selecting magnets and a sample of events were recorded on tape. With this information, this background can be estimated as follows:

1) The total number of triggers was found to be 30745 during the +165 GeV exposure.The protons on target corresponding to the above number of events was P.O.T.$=1.51 \times 10^{18}$.

2) The total number of triggers with beam monitor data while the iron plug was placed in front of the beam was 2717 with a corresponding number of protons on target of 1.88×10^{17}

3) Only one event passed the quasi-elastic criteria while the plug was in the beam.

With the above information, one can estimate the background over the

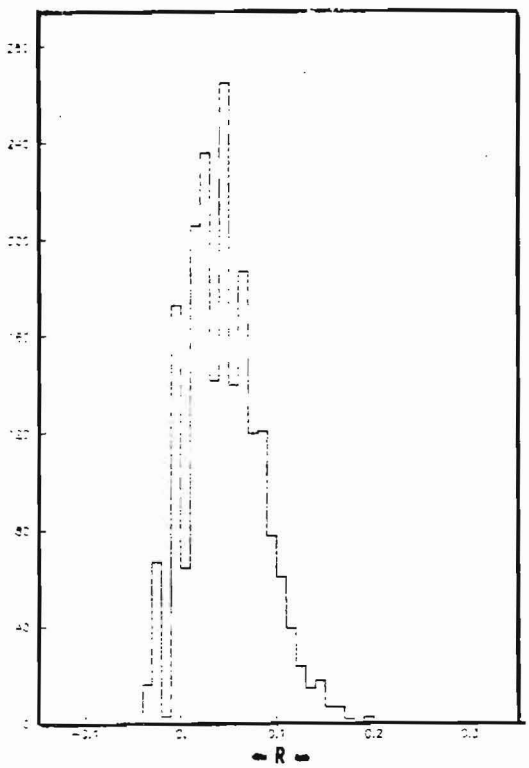

figure 23

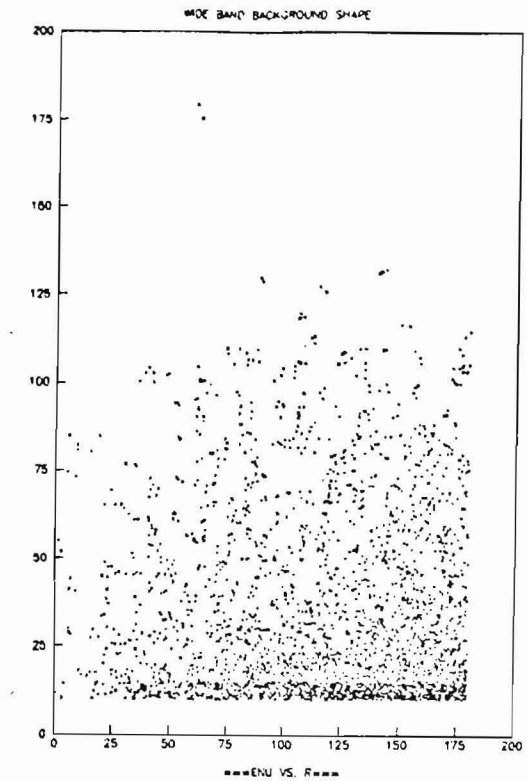

figure 24

entire E vs R space to $\frac{1.51\times10^{18}}{1.88\times10^{17}}\times 1 \approx 8$ events. Normalizing to the number of events that passed the quasi-elastic event criteria in the -165 Gev sample gives $\approx$ 1.9%. The error is estimated from a 68%confidence interval with Poisson stadistics. This gives $1.9^{-3.8}_{+.60}\%$. Clearly the statistical error is large so a better estimate is taken from the Monte Carlo beam simulations. The beam Monte Carlo estimate is 1.44%which is in agreement with this and other experiments. In order to determine the signal and background efficiencies, the spectrum of this events is simulated from the Beam Monte Carlo. Quasi-elastic events are generated and analysed to find $\epsilon^{s}_{wbb} = .25\%$ and $\epsilon^{b}_{wbb} = .89\%$.

The same analysis is done in the +165 Gev exposure. In this case the

background estimate from this data is $.46\%^{1.1\%}_{-.1\%}$ and the beam Monte Carlo estimate is .97%. The signal and π-band efficiencies are found to be $\epsilon^{s}_{wbb} =$ .17% and $\epsilon^{b}_{wbb} =$ .60% This background is negligible in both the +165 Gev and -165 Gev exposures but it is included in the calculation of R for completness.

INVERSE MUON BACKGROUND from $\nu_\mu + e \rightarrow \nu_e + \mu$

Because of the dynamics of the interaction $\nu_\mu + e \rightarrow \mu + \nu_e$, the muon from these events are predominantly at low energy and thus they can populate the $y > .6$ signal region. These events are identified with a cut on $E_\mu \theta^2_\mu < 3$ MeV and are subtracted from the signal region[28].

The next table, is a summary of the rest of the numbers needed to determine the upper limit on R

$BEAM$	$\pi - BAND$	$SIGNAL\ \ REGION$
$(\overline{\nu}_\mu)$	$DATA: 407 events$	$DATA: 2 events$
$-165\ \ GeV$	$\epsilon^{B}_{Q} = 0.825$	$\epsilon^{s}_{Q} = 0.0019$
	$\epsilon^{B}_{\tau} = 0.245$	$\epsilon^{s}_{\tau} = 0.119$
(ν_μ)	$DATA: 330$	$DATA: 3$
$+165\ \ GeV$	$\epsilon^{b}_{Q} = 0.830$	$\epsilon^{s}_{Q} = 0.004$
	$\epsilon^{b}_{\tau} = 0.238$	$\epsilon^{s}_{\tau} = 0.119$

Finally, all the above numbers are combined to calculate the 90%cofidence level upper limit on R called $R_{90\%}$. The results are given in the next table where $R_0 = R|_{observed}$.

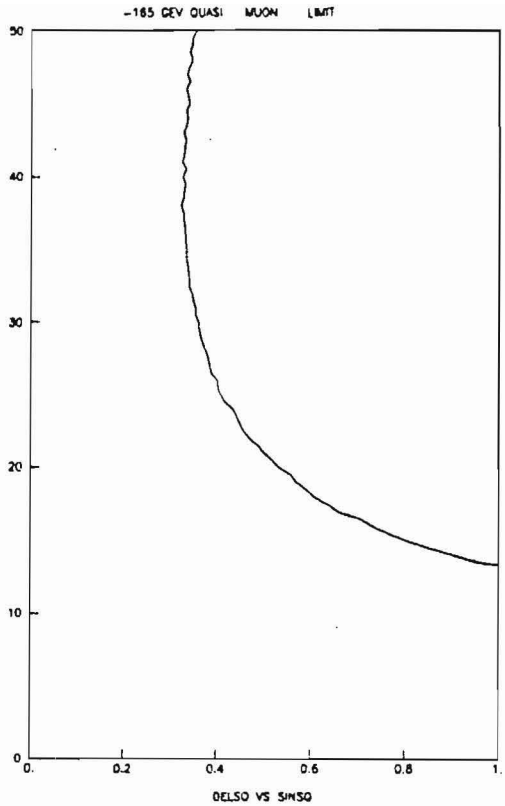

figure 25

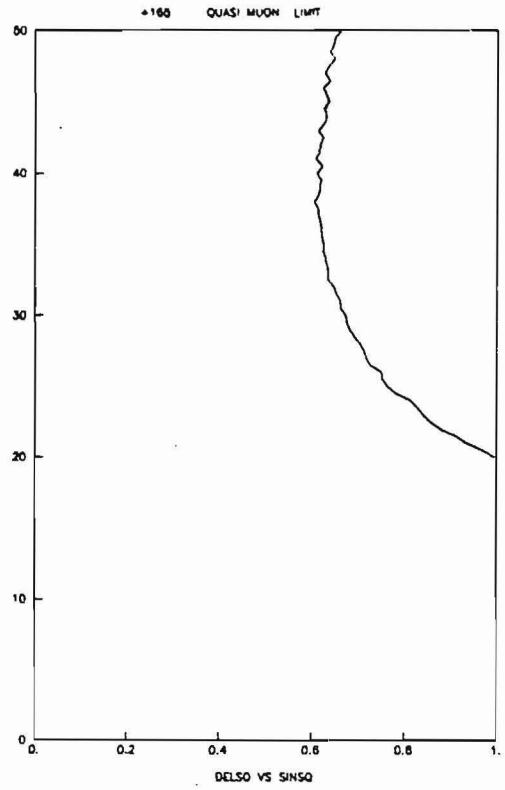

figure 26

$BEAM$	R_0	$R_{90\%}$
$(\overline{\nu}_\mu)$	-0.0030	0.046
ν_μ	0.0166	0.086

Having found the ratio $R_{90\%}$ the upper limit on δ^2 can be found from:

$$R_{90\%} = \frac{\int \Phi(E_\nu) P(\nu_\mu \rightarrow \nu_\tau) \frac{d^2\sigma^\tau}{dE_\nu dq^2} \quad dE_\nu dq^2}{\int \Phi(E_\nu) \frac{d^2\sigma^\mu}{dE_\nu \, dq^2}} B.R. \qquad V.1$$

Where $\frac{d^2\sigma^{\tau,\mu}}{dE_\nu dq^2}$ is the quasi elastic cross section for τ, μ respectively, $\Phi(E_\nu)$ is the neutrino flux, $P(\nu_\nu \rightarrow \nu_\tau)$ is the oscillation probability previously given and $B.R.$ is the branching ratio $= .18$ for the leptonic decay of $\tau \rightarrow \mu + \nu_\mu + \nu_\tau$. [16]

The above expression is solved numerically in terms of the mixing angle θ and the mass squared difference δ^2 at the experimentally found $R_{90\%}$. The

result is shown in figures 25 and 26 for the anti-neutrino run $\overline{\nu}_\mu$ at -165 GeV train energy and for the neutrino run ν_μ at +165 Gev. The upper limit on the mass squared difference in this channel is $\delta_{90\%} = 15$ eV^2 and $\delta^2_{90\%} = 20$ eV^2 for $\overline{\nu}_\mu \rightarrow \overline{\nu}_\tau$ and $\nu_\mu \rightarrow \nu_\tau$ respectively at full mixing angle, $\theta = \frac{\pi}{4}$.

SENSITIVITY OF $R_{90\%}$

The sensitivity of the $R_{90\%}$ to the measured and calculated quantities is given here. The following table shows the dependence of $R_{90\%}$ to the number of observed data events keeping the rest of the quantities fixed:

$R_{90\%}$	N_s
0.046	2
0.072	3
0.100	4

Keeping the number of observed events at N_s=2 and changing the ϵ^s_Q results in:

	$R_{90\%}$	ϵ^s_Q
	0.046	0.0019
$N_s = 2$	0.066	0.000
	0.032	0.0038

Changing ϵ^s_τ yields:

	$R_{90\%}$	ϵ^s_τ
	0.046	0.119
$N_s = 2$	0.036	0.155
	0.072	0.083

The upper limit on $\delta^2_{90\%}$ will change proportionally with the $\sqrt{R_{90\%}}$. Thus

if the observed number of events was 4 instead of 2 the $\delta_{90\%}$ upper limit for $\overline{\nu}_\mu \rightarrow \overline{\nu}_\tau$ will change from 13 eV^2 to 19 eV^2 at full mixing angle.

VI. *ELECTRON CHANNEL – ANALYSIS –*

In this analysis, all events recorded that pass a special trigger condition during the 1982 run at -165 GeV, +165 GeV, 200 GeV, 250 GeV are considered. The trigger condition was $PTH \equiv M > 2 \quad planes \otimes \sum\sum \otimes N > 1 \quad channel > 1 \quad chamber \otimes (muon \quad veto)$. The components of this trigger have been defined in the calorimeter section. This trigger was measured to be $\approx 100\%$ efficient down to shower energies $E_h \approx 5 \quad GeV$ for both charged and neutral current events.

Among the events that passed the PTH trigger condition, the interaction of a $\nu_\tau + N \rightarrow \tau + N^*$, where N^* describes a nucleon or a low energy excited state of the nucleon (similar to the N^* in the Muon Channel section), with the produced τ decaying into $e + \nu_\tau + \nu_e$ is searched for. The signature of this interaction in the calorimeter is a single electromagnetic shower of low energy and low transverse momentum. Because of the large neutral current background, energy and transverse momentum cuts are not sufficient to isolate this events. A filter to discriminate neutral current hadron showers from electromagnetic showers is needed. From scans of electron showers and hadron showers, it is found that the electron showers are thin, dense and do not have visible tracks around them. These features are quantified with the following definitions:

$$w = l(\tan\theta_1 - \tan\theta_2) \qquad VI.1$$

$$\rho = \frac{n}{a}, \quad with \quad a = wl \qquad VI.2$$

Where "w" is the width of a shower, "ρ" is the densitity of a shower and "a" is the area of a shower; l is the length of the shower, defined as the distance downstream of the vertex of the interaction corresponding to a shower containment of $\approx 98\%$, θ_1 and θ_2 are angles measured with respect to the neutrino direction adjusted so that 70%of the total shower hits n is contained inside the cone formed by θ_1, θ_2 and the length l of the shower. See figure 27.

The vertex of the shower is found from the flash chamber hits with pattern recognition programs. The longitudinal vertex coordinate is found by a downstream search of flash chamber hits within an adjustable window. (This window normally narrows as the vertex is approached). The search stops when no hits are found. This condition determines the longitudinal coordinate of the vertex. The perpendicular coordinate on each flash chamber view is a result of a fit to the last 32 downstream chambers using the centroids of the hits weighted by the σ^2 of the hits within the window.

The width w and the density ρ are calculated the X-Y-U flash chamber views and the average density $\overline{\rho} = \frac{\rho_x+\rho_y+\rho_u}{3}$ and the average width $\overline{w} = \frac{w_x+w_y+w_u}{3}$ is calculated. The third quantity used in the electromagnetic filter is the number of tracks around the shower "$nbox$". This quantity is defined

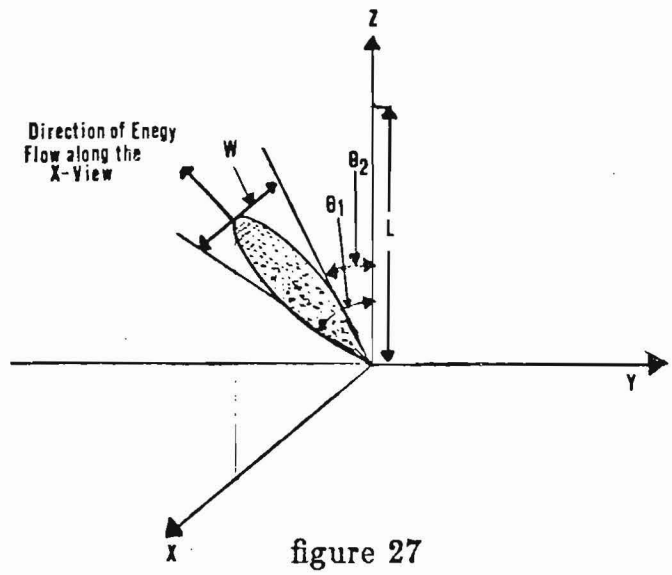

figure 27

via the following procedure:

1)The shower is enclosed in a region of area A=l×d where l is the length of the shower and d is perpendicular to l. d is not shown in figure 27. It is a line of a fixed length chosen to contain all of the shower hits.

2)All the hits that have near neighbors (ie. all the hits in the shower core) are removed.

3)All of the hits left inside the area A after removing the shower core are added.

4)The same process is repeated for each flash chamber view and the total hits for each of the flash chamber views are added.

The number of hits left is a measure of the extent to which the shower

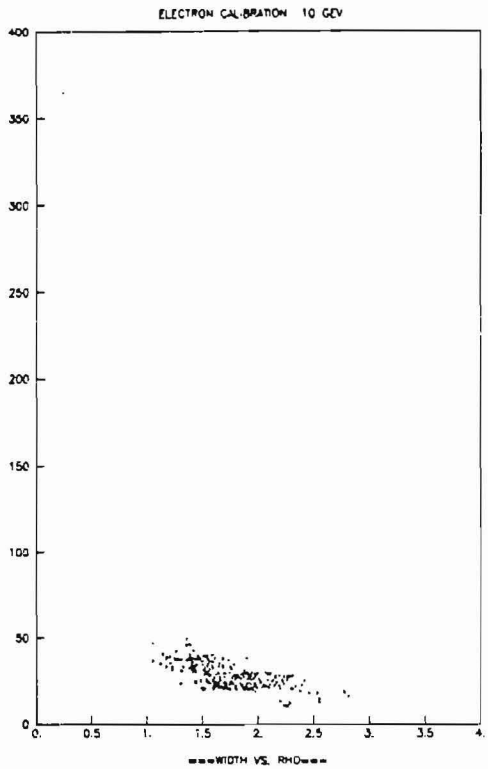

figure 28

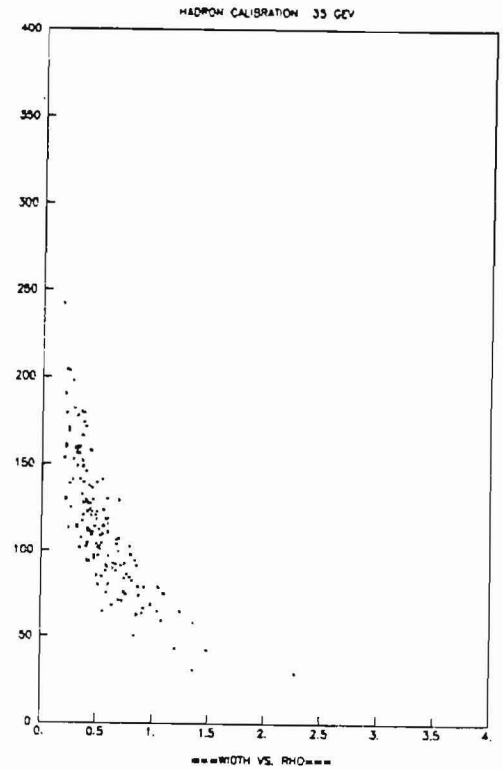

figure 29

is accompanied by a halo of single tracks.

This filter is tested with electron and hadron calibration data. Figures 28 and 29 are scatter plots of w vs. ρ for electron calibration events at 10 GeV and hadron calibration events at 35 GeV. We see from these plots that as expected electron showers are denser and thinner than hadronic showers. We set the cuts at w=50 (arbitrary units) and ρ =.98 (arbitrary units). With these cuts, the number of hadron events left N^H_{left} as a function of energy is summarized in the following table:

E	N_{total}	N^H_{left}	$RATIO = \frac{N^H_{left}}{N_{total}}$
10 GeV	223	8	0.04
20	265	9	0.03
35	157	3	0.02
50	418	1	0.002
75	146	1	0.0068
100	204	0	0.00
120	175	0	0.00

The number of electron events left N^e_{left} as a function of energy is summarized:

E	N_{total}	N^e_{left}	$RATIO = \frac{N^e_{left}}{N_{total}}$
5 GeV	79	79	0.96
7.5	155	156	0.99
10	277	277	1.0
15	277	277	1.0
20	207	207	1.0
35	63	63	1.0

The next step is to run this filter on all the data. Since the filter is not 100%efficient to reject hadron showers at all energies, it is necessary to make a background subtraction. After this subtraction, the number of events left will determine whether or not we have a signal. This number is given by:

$$n_e = nc - f(cc) \qquad VI.3$$

Where nc is the number of muonless events, cc is the number of events with a

muon and f is the ratio of neutral to charge current events without the filter requirement.

The presence of the muon and its associated hits in the charged current events will bias this subtraction therefore the muon hits must be eliminated before the filter selection. The following steps are taken to find an unbiased algorithm to remove muon hits:

STEP1: Find the muon track in a particular charged current event. Count the hits corresponding to this muon track inside a road of ± 5 cm from the end of the shower to the exit point of the muon in the calorimeter. Store these hits.

STEP2: Find a sample of neutral current events with energies in the range $5\text{GeV} < E_h < 20\text{GeV}$. This region is considered to be the region where the muon hits can severely bias the filter measurements. Predict the angle at which a muon would have emerged if the event was a charged current event. This can be calculated in the Dichromatic Beam Exposure from the knowledge of the average beam energy, shower angle and shower energy.

STEP3: Superimpose the hits on the neutral current event from the vertex up to the exit point of the muon track in the calorimeter.

With these fake charged current events, the filter bias (if any) as a function of how the muon hits are removed, can be tested. But first, the muon multiplicities (to be defined shortly) are looked at in the regions where the shower hits overlap with the muon hits and also in the region away from

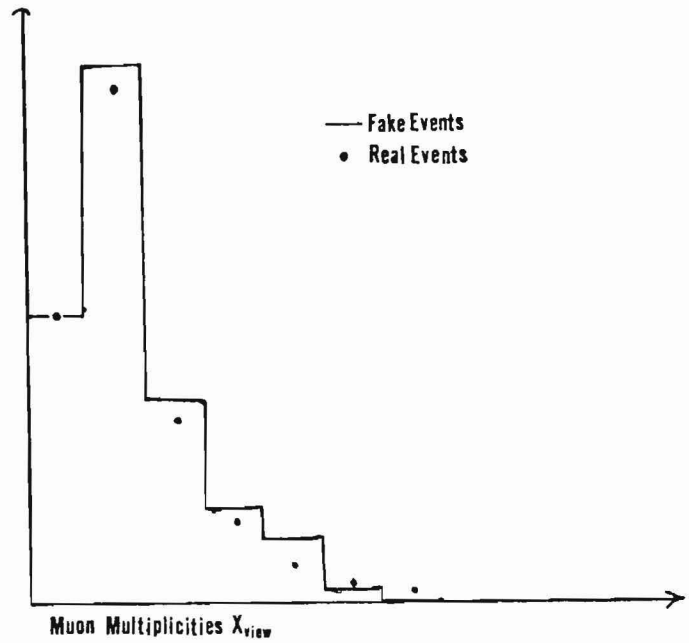

figure 30

the shower hits. The region of overlap is called "*inside*" the shower. It is the region between the vertex of the interaction and the end of the shower determined by its length l. The region "*outside*" of the shower is defined as the region from the end of the shower til the point in the calorimeter where the muon exits. A road of ± 20 clock counts $\approx$ 10 cm wide is placed along the muon track. The hits of each chamber are projected along this road into a one dimensional histogram. These distributions are called muon multiplicities.

The resulting histogram is shown in figure 30 for the region inside the shower along the X flash chamber view. Also superimposed in the figure is the muon multiplicity for real charged current events. One can see that

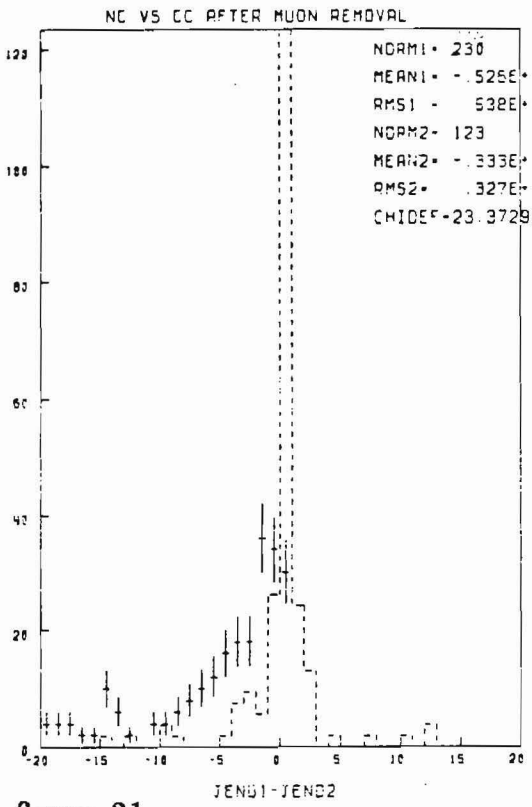

figure 31

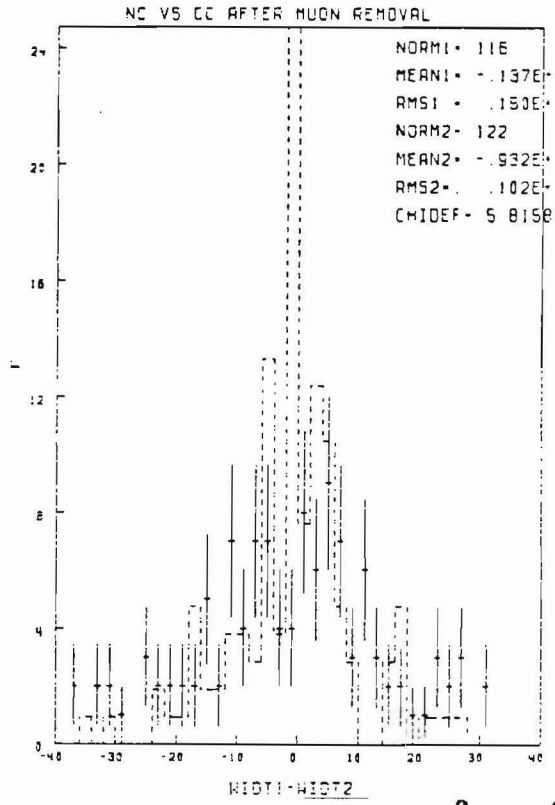

figure 32

the two distributions are in agreement. The muon multiplicities are also in agreement in the region outside of the shower but this is not relevant here since nothing was done to the muon hits in this region during superposition of the events and all of the muon hits are removed during the filtering process.

These events are analysed and the algorithm to remove the muon and calculate the shower length is adjusted till the distributions of $\Delta l = l_{nc} - l_{fake}$, $\Delta w = w_{nc} - w_{fake}$ and $\Delta \rho = \rho_{nc} - \rho_{fake}$ are all consistent with zero. This insures that there is no bias. Figures 31,32,33 show distributions of these Δ variables. Also shown in figures 34,35,36,37 are comparizons of $nbox$, ρ, l, of nc events and real cc events after muon removal.

After filtering the data, kinematical cuts are imposed on the sample. It

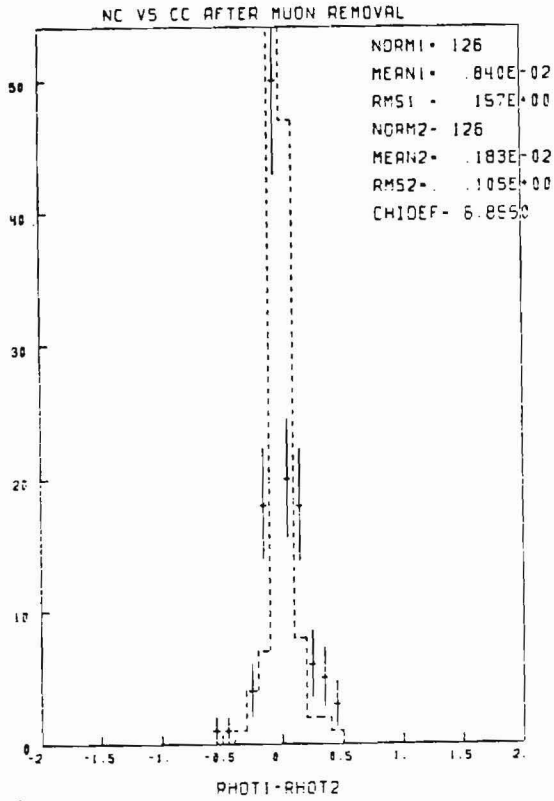

figure 33

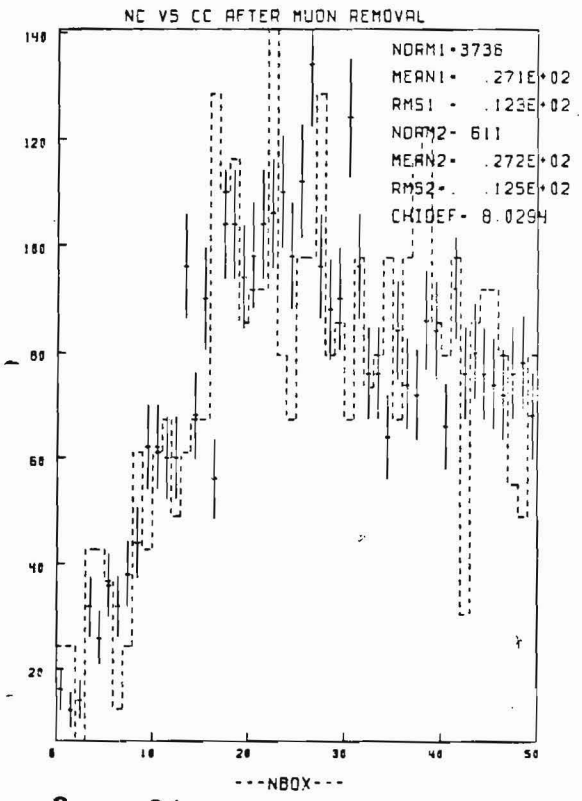

figure 34

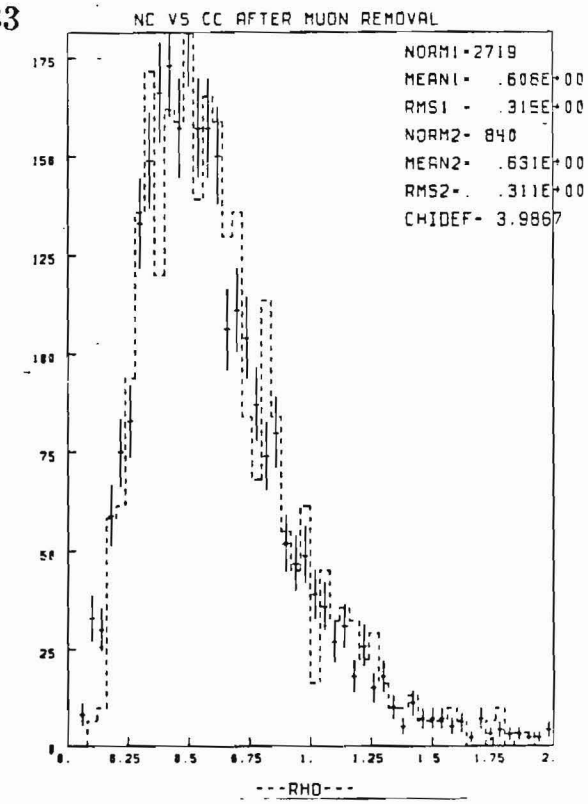

figure 35

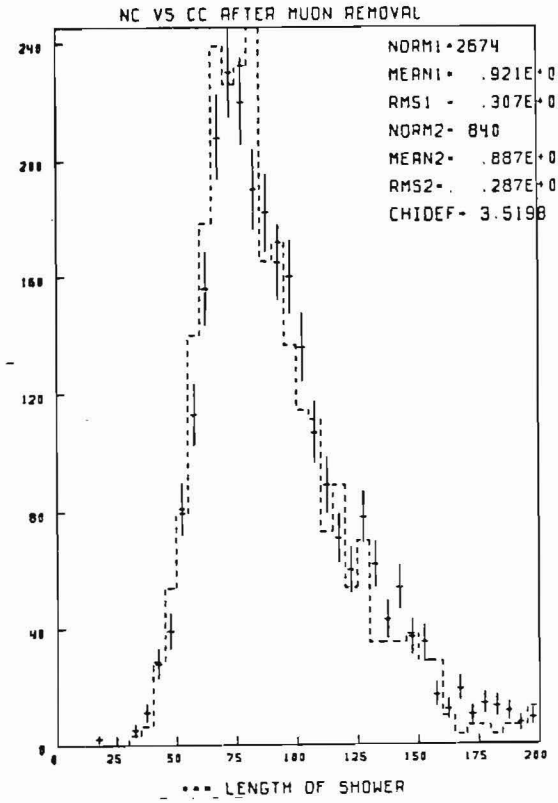

figure 36

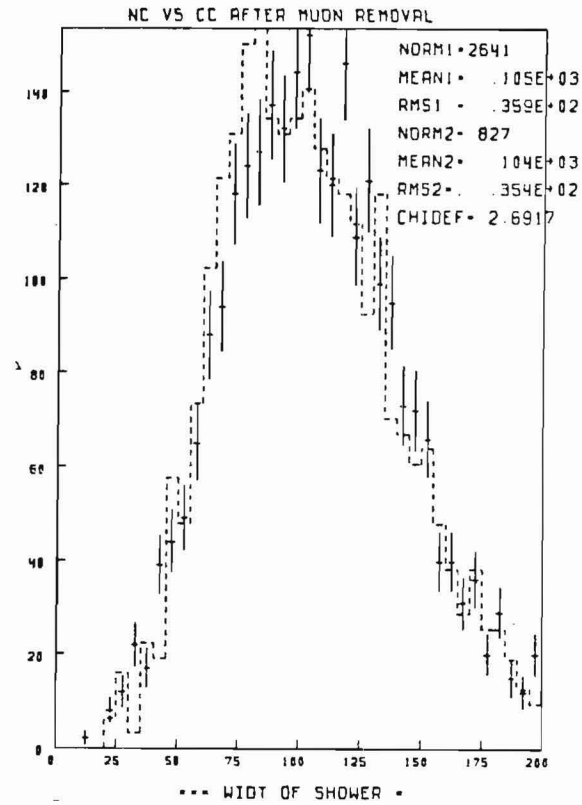

figure 37

is required that the visible energy of the shower be $E_h > 10$ GeV to remove trigger bias effects on the number of charged currents events versus neutral current events. It is also required that the transverse momentum of the showers with respect to the neutrino direction p_t , be less than 2 GeV and that $y = \frac{\nu}{E_\nu}$ be less than .8. It is found from Monte Carlo simulation of a $\nu_\tau + n \rightarrow \tau + n$ with the $\tau \rightarrow e + \nu_\tau + \nu_e$ that these two latter cuts retain 98%of the events while further reducing the neutral current background. The sample obtained upon imposition of the above mentioned cuts are outlined below. With cuts on $E_h > 10$ GeV, $radius < 120$ cm, $y < .8$:

Train Energy	*cc events*	*nc events*	$f^{-1} = \frac{nc}{cc}$
$-165Gev$	3295	1283	$2.57 \pm .08$
$+165GeV$	4861	1562	$3.11 \pm .09$
$+200GeV$	2740	722	$3.25 \pm .14$
$+250GeV$	2346	722	$3.25 \pm .14$

After imposing the selection criteria and the requirement that $p_t < 2$ GeV the number of events left from the above sample is :

Train Energy	*cc events*	*nc events*
$-165Gev$	63	24
$+165GeV$	56	26
$+200GeV$	39	12
$+250GeV$	23	9

An estimate of the ratio R of ν_τ to ν_μ events in this channel can be found from the above samples througth the relation:

$$n_e = n_\tau \epsilon_e = n_q^t \epsilon_e R \qquad VI.4$$

Where n_q^t is the number of events that passed the quasi-elastic criteria in the muon channel section corrected for electronic efficiency and acceptance, ϵ_e is the Monte Carlo efficiency for finding an electron produced from the decay of the τ in a quasi-elastic ν_τ interaction, n^τ is the number of ν_τ events in this channel. Equating this expression with equation VI.4 one gets:

$$R = \frac{1}{\epsilon_e n_q^t}(nc - fcc) \qquad VI.5$$

The distribution of R, $P(R)$ can statistically be reconstructed and the upper limit can be found from the condition $.10 = \int_{-\infty}^{R_0} P(R)dR$ in analogy with the MUON CHANNEL analysis but it is found that in this case, the distribution $P(R)$ is well appoximated by a gaussian; therefore, an accurate and convinient expression is given here. First propagate errors:

$$\delta R = \frac{1}{\epsilon_e n_q^t}(\delta(nc) - f\delta(cc)) \qquad VI.6$$

Square and take the mean of the above:

$$\overline{(\delta R)^2} = \frac{1}{(\epsilon_e n_q^t)^2}\overline{(\delta nc)^2} + f^2\overline{(\delta cc)^2}) \qquad VI.7$$

Using the fact that $\overline{(\delta nc)^2} = nc$ and $\overline{(\delta cc)^2} = cc$ and defining $\sigma_R = \sqrt{\overline{(\delta R)^2}}$ gives:

$$\sigma_R = \frac{1}{\epsilon_e n_q^t}\sqrt{(nc + f^2 cc)} \qquad VI.8$$

The confidence level upper limit on R can be found from the following relation:

$$R_{90\%} = R_0 + 1.28\sigma(R) \qquad VI.9$$

The above relation is graphically shown in figure 38 where R_0 is the particular R evaluated at the observed quantities $R_0 = \frac{1}{\epsilon_e n_q^t}(nc - fcc)|_{observed}$.

The following table is a summary of the final quantities needed in the determination of $R_{90\%}$:

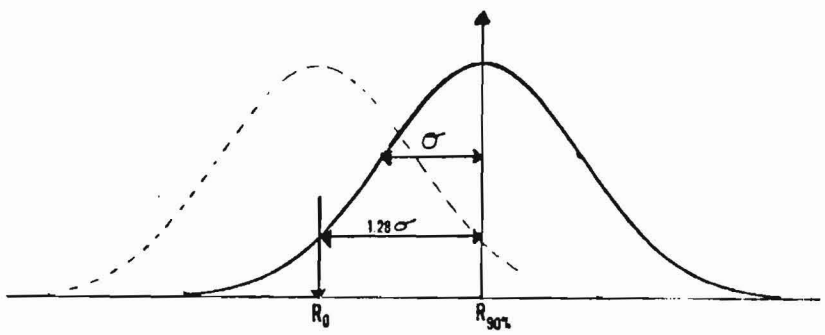

figure 38

TRAIN	*ENERGY*	n_q^t	ϵ_e
	$-165GeV$	482	0.625
	$+165GeV$	392	0.625
	$+200GeV$	191	0.644
	$+250GeV$	212	0.666

If we interpret the above results as due to neutrino oscillations, we can get a limit on the probality $P(\nu_\mu \rightarrow \nu_\tau)$ througth:

$$R_{90\%} = \frac{\int \Phi(E_\nu) P(\nu_\mu \rightarrow \nu_\tau) \frac{d^2\sigma^\tau}{dE_\nu dq^2} \quad dE_\nu dq^2}{\int \Phi(E_\nu) \frac{d^2\sigma^\mu}{dE_\nu\, dq^2} dE_\nu dq^2} B.R. \qquad VI.10$$

Where: $\Phi(E_\nu)$ = neutrino flux, $P(\nu_\mu \rightarrow E_\tau) = \sin^2 2\theta \sin^2 \frac{1.27\delta^2 l}{E_\nu}$, $\delta^2 = |m_1^2 - m_2^2|$, $\frac{d^2\sigma^{\tau,\nu}}{dE_\nu dq^2}$ is the quasi- elastic cross section for τ and μ respectively and $B.R.$ is the branching ratio for the decay of the $\tau \rightarrow e + \nu_\tau + \nu_e$.

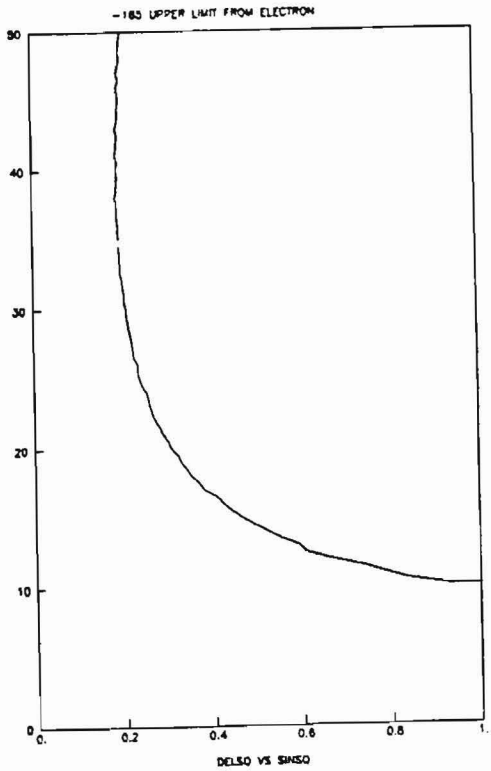

figure 39

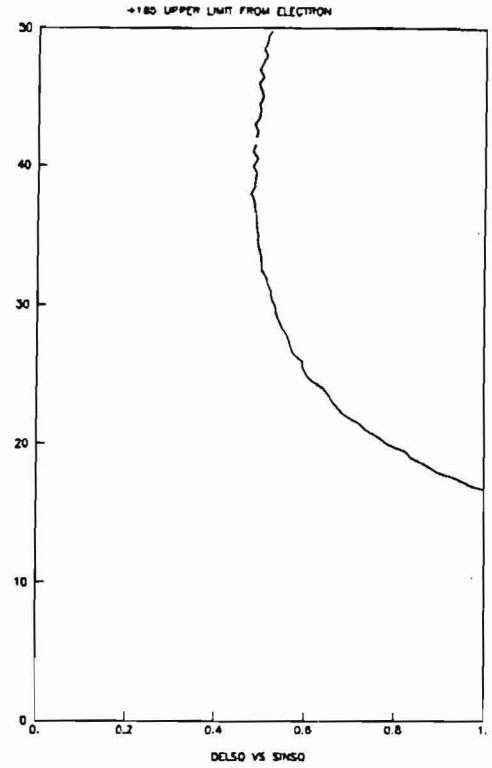

figure 40

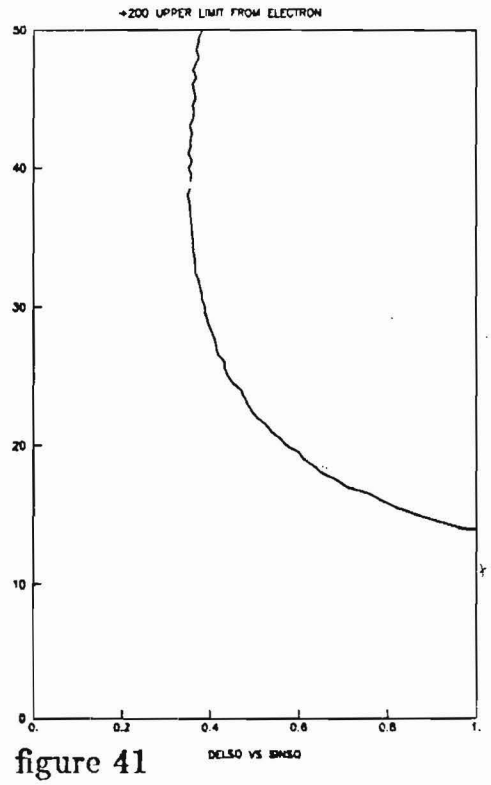

figure 41

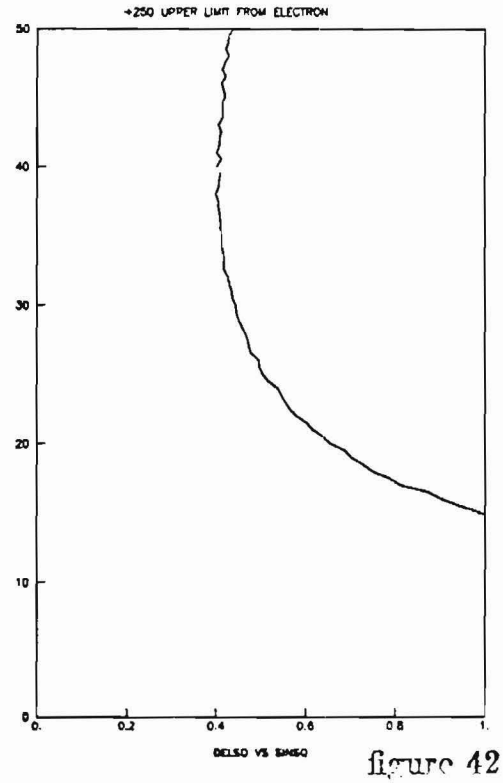

figure 42

The above quantity can be calculated numerically in terms of the mixing angle θ and the mass squared difference δ^2. The results are shown in figures 39, 40, 41, 42. The following table is a summary of the results:

TRAIN	*ENERGY*	R_0	$R_{90\%}$	$\delta^2_{90\%}(\theta = \frac{\pi}{4})$
-165	GeV	-0.00171	0.0258	10 eV^2
$+165$	GeV	0.0326	0.0656	17 eV^2
$+200$	GeV	-0.00035	0.0481	13 eV^2
$+250$	GeV	0.0149	0.0552	15 eV^2

SENSITIVITY of $R_{90\%}$

The sensitivity of the $R_{90\%}$ to the measured and calculated quantities that enter in the calculation of $R_{90\%}$ is studied here. The following table illustrates the dependence of $R_{90\%}$ to the number of observed events nc after all cuts keeping the rest of the quantities fixed:

nc	$R_{90\%}$
24	0.0258
26	0,0331
28	0.0404
30	0.0478
40	0.0841
50	0.120

The dependence on the efficiency determined from the Monte Carlo is given in the next table keeping $nc = 24$ and $cc = 63$:

ϵ_e	$R_{90\%}$
0.625	0.0258
0.500	0.0368
0.400	0.0460
0.300	0.0613
0.200	0.09120

The upper limit $\delta^2_{90\%}$ will change proportionally with the $\sqrt{R}_{90\%}$. Thus if the number of *nc* events was 40 instead of 24, the upper limit on $\delta^2_{90\%}$ would change from $\approx$10 eV^2 to $\approx$18 eV^2

VII. *COMPARISON WITH OTHER EXPERIMENTS*

From the derivation on neutrino oscillation, one sees that neutrino oscillations can take place if: 1) the weak eigenstates are linear combinations of mass eigenstates, (which implies that lepton number is not strictly conserved) and 2) at least two eigenstates have different masses. We find that the probability distributions for the case of two mass eigenstates are given by:

1) $P(\nu_\alpha \rightarrow \nu_\alpha) = 1 - \sin^2 2\theta \sin^2(1.27 \frac{\delta^2 L}{E_\nu})$

and

2) $P(\nu_\alpha \rightarrow \nu_\beta) = \sin^2 2\theta \sin^2(1.27 \frac{\delta^2 L}{E_\nu})$

where ν_α and ν_β are any two neutrino flavors. The rest of the quantities have been defined in section...

The two solutions, correspond to two very different kinds of experiments. Solution 1) corresponds to inclusive (or disappereance) experiments; solution 2) corresponds to exclusive (appearence) experiments.

EXCLUSIVE OSCILLATION LIMITS

In the exclusive (or appearence) search, an experiment searchs for an anomalous number of some neutrino type ν_α in a relative pure neutrino source of another type ν_β. From the number of observed excess events relative to the number predicted events, different experiments can set limits on $P(\nu_\alpha \rightarrow$

ν_β).

The sensitivity of these type of experiments are determined by:

1)Background rate of expected events.

2)Observed rate of excess events.

3)$\frac{L}{E_\nu}$ large but with a reasonable number of events left in the sample. (As the number of events goes down, the posible restrictions on the mixing angle are lowered)

The best limits at this time on this type of experiment on $\nu_\mu(\overline{\nu_\mu}) \rightarrow \nu_\tau(\overline{\nu_\tau})$ oscillations are: (see also reference 31)

	$\delta^2_{90\%}$ at $\sin^2 2\theta = 1$		EXPERIMENT
$\nu_\mu \rightarrow \nu_\tau$	3	eV^2	$E532 - FNAL^{(29)}$
$(\overline{\nu}_\mu) \rightarrow \overline{\nu}_\tau$	2.2	eV^2	$ITEP - FNAL - MICH^{(30)}$
$\nu_\mu \rightarrow \nu_\tau$	17	eV^2	THIS EXPERIMENT
$\overline{\nu}_\mu \rightarrow \overline{\nu}_\tau$	10	eV^2	THIS EXPERIMENT

INCLUSIVE OSCILLATION LIMITS

In order to do this type of experiment, the change in the number of a given type of neutrinos ν_α with energy E_ν or distance L must be measured.

Measurements of neutrino rates as a function of energy E_ν can in principle yield the same results as measurements made at different distances frome the production source L. However, an experiment that attempts to measure the oscillation distribution as a function of energy is subject

to the uncertainties in the measurements of the absolute source rate and spectrum at the detector. To circumvent this problem, two experiments: one at Fermilab[32] and one at CERN PS[33] have been designed to measure neutrino rates at two different lengths L_1 and L_2 from the neutrino source. Figures 37 and 38 show the results of these two experiments. CCFR experiment excludes to the 90% C.L. oscillations of muon neutrinos into any other type of neutrino in the range of $30 < \delta^2 < 900$ eV^2 for $\sin^2(2\theta) > 0.03$-0.015. The CDHS CERN PS experiment excludes a range $.3 < \delta^2 < 90$ eV^2. This lattest result significantly improves the $\nu_\mu \rightarrow \nu_\tau$ oscillation limit $\delta^2 < 3$ eV^2 in the exclusive type experiment.

	$\delta^2_{90\%}$	E_ν	L_1	L_2	*EXPERIMENT*
	$\sin^2 2\theta = 1$	(GeV)	(mts)	(mts)	
$\nu_\mu \rightarrow \nu_x$	$30 \quad eV^2$	$30 \quad to \quad 230$	885	1286	$CCFR^{(32)}$
$\nu_\mu \rightarrow \nu_x$	$.3eV^2$	$< E_\nu > \approx 3GeV$	130	880	$CDHS^{(33)}$

VIII. *CONCLUSIONS*

Experiments after the report of a positive result on neutrino oscillations by the Savannah River reactor[34] group, have failed to confirm such result. At present, there is no conclusive evidence for neutrino oscillations. Accelerator experiments have excluded mixing angle and neutrino mass regions but there remains still larger regions to be explored. Our experiment, using experimental methods independent of previous experiments, sets an upper limit confidence level of $\delta^2_{90\%} = 10.\text{eV}^2$ at full mixing in a -165 Gev $\overline{\nu}_\mu$ exposure. This confirms the results of other exclusive type experiments. Future experiments, should be planned to be sensitive to masses and mixings about an order of magnitude below the present limits of exclusive and inclusive type experiments. In particular, the very stringent limits from CERN CDHS[33] should at least be reconfirmed in different experimental setups where systematics and acceptances are different.

It is also noted that, at present, there is no strong theory on the very basic problem of lepton masses and also on the possibility that they mix. Setting the scale of these measurements and mixing is a problem with little theoretical guidance and therefore measurements should continue probing even further into the unexplored regions.

IX. ACKNOWLEDGEMENTS

I am forever gratefull to my advisor Larry Rosenson for his constant encouragement and guidance during the course of this work. I also wish to thank him for his moral support and leniency during bad times that i together with my family had to endure during the past years due to circumstances unrelated to this work but that greatly affected my life.

I am forever gratefull to Tommy Lyons for his innumerable contributions during the construction and the design of this detector. Without his insights, the construction as well as the operation of this detector would have been much harder. I also wish to thank him for the confort that he and his family gave me during my stay at Fermilab.

I wish to thank Jerome Friedman for the many enlightening physics conversations and help during the early developments of the analysis of this data. He has been an advisor to all of us.

Many thanks to our spokesmen Frank Taylor and Jimmy Walker for their constant drive needed to get this experiment done. To Frank Taylor, I also wish to thank him for his constant effort to understand and keep the overall experiment in one piece.

Many thanks to Maury Goodman for his efforts to put together and keep together the off-line analysis library.

The succes of the muon tracking package is due to the perseverance of Robin Verdier in the development of the software needed to do this task. I also wish to thank the many contributions made by Scott Whitaker in this subject.

Many thanks to Stue Fuess for his work done to align the detector and understand the many aspects of the calibration of the calorimeter.

The understanding of this beam at Lab C comes from in part to the efforts of Ray Brock, Dan Owen, Randall Pitt, Linda Study and Harry Weerts. I wish to thank Harry Weerts for the quick development of part of the beam software needed in the analysis of this experiment.

The author also acknowledges the early contributions of Dixon Bogart in the development of a large part of the flash chamber readout and Linda Stutte in the on-line data adquisition software.

Thanks to Ron Olsen and friends for the technical support given in the construction of this experiment. Special thanks to Sammy Rumple for her patience in the stringing of the proportional tubes.

To my fellow graduate students: Terry Eldridge, Rich Magahiz, Asset Mukherjee, Tom Mattison, Mike Tartaglia and Gong Ping Yeh; i wish to thank for the enormous work that they have put into this experiment and for their friendship. I will always remember the dinner times and other times we had around the Fermilab boundaries while at least one of us was on shift or fixing the apparatus.

Finally, i wish to thank all members of the E594 collaboration that contributed to the succes of this experiment and also to the Fermilab staff for providing a beam and all the hardware and software needed to accomplish this work.

X. REFERENCES

1)B. Pontecorvo: Zh. Eksp. Teor. Fis. 33, (1957), 549; B. Pontecorvo, JETP (Sov. Fiz.) 53 (1967)1717.

2) The current "standard model" of weak and electromagnetic interactions based on spontaneously broken $SU(2)_L \times U(1)_Y$ gauge symmetry was proposed by S. Weinberg, Phys. Rev. Lett. 19, 1264(1967) and by A. Salam, Elementary Particle Theory: Relativistic Groups and Analycity (8th Nobel Symposium), edited by N. Svartholm, Almquist and Wiksell, Stockholm, 1968.

3) For a review of θ_W: A. Sirlin and W. Marciano, Nuclear Phys., B189, 442(1981).

4) A Fresh Look at Neutrino Oscillations, Ref. TH. 2788-CERN,november 1979.

5) Quantum Mechanics of Oscillations can be found in: Boris Kayser, SLAC-PUB-2685, february 1981.

6) N. W. REAY, talk at Proceedings of the 1983 International Symposium on Lepton and Photon Interactions at High Energies. Cornell University August 4-9, 1983.

6) M. Jonker et al., CHARM Collaboration, Phys. Lett., 96b, 435.

7) H. Abramovicz et al.,CDHS collaboration, Z. Phys. C13(1982)179.

8) P.O. Hulth, Neutrino 81, Maui, Hawaii(1981).

9) P. Fritze et al., Abclos collaboration, Phys Lett. 96B,427(1980).

10) K. Winter, Procedings of the 1983 International Symposium on Lepton and Photon Interactions at High Energies, Cornell University, August 4-9, 1983.

11)DELCO collaboration,W. Bacino et al.,Phys. Rev. Lett.43, 1073(1979).

12) Mark II collaboration,R.H. Schindler et al., Phys. Rev. D 24, 78(1981).

14) C.H. Albrigth, Robert Shrock, J. Smith, Tests for Observing Tau Neutrino Interactions in a Beam Dump Experiment.(unpublished?)

15) Interpretation of beam dump experiments can be found in: E.L. BERGER, L. CLAVELLI and N.R. WRIGHT Physical Review D, Volume 27, Number 5, 1 March 1983.

16)Particle Data Group, Review of Particle properties, Phys. Lett. 111B1 (1982)1.

17) Blocker C.A. et al., Phys. Rev. Lett. 48 (1982)1586.

18) C.H. Llewellin Smith, Physics Reports 3, no.5 (1972)261-379.

19) Phenomenology on Neutrino Reactions, L.M. Sehgal, ANL-HEP-PR-75-45.

20)Physical Review D, Volume 28, Number 3, 1 August 1983.

21) τ lifetime: MARK II result $\tau = (3.20^{+}-0.41^{\pm}0.35) \times 10^{-13}$ and TASSO result $\tau = (1.9^{\pm}1.4) \times 10^{-13}$ sec have deen quoted from private coomunications during the 1983 International Symposium on Lepton and

Photon interactions at High energies Cornell University.

22) E.D. Commins, Weak Interactions (Mc Graw-Hill advanced physics monograph series).

23) Michel, L. Proc. Phys. Soc. (London), A63:514 1950.

24) Bouchiat., C., and L. Michel: Phys Rev, 106:170(1957).

25) IEEE Transactions on Nuclear Science, Vol. NS-29, No.1, February 1982

26) Dan. Owen survey of the beam.

27) IEEE Transactions on Nuclear Science, Vol. NS-29, No.1, February 1982.

28) Inverse Muon: M. Jonker at al, Phys. Lett., 93B, (1980)203.

29) Best limit on $\nu_\tau \rightarrow \nu_\mu$; E531-FNAL N. USHIDA et al., Phys. Rew. Lett. 47,1694(1981)

30) Best limit on $\overline{\nu}_\mu \rightarrow \overline{\nu}_\tau$: A.E. Asratyan et al., Phys. Lett. 105B, 301(1981).

31) Upper limit on $\nu_\mu \rightarrow \nu_\tau$: Volume 47, Number 22, Physical Review Letters, 30 November 1981,1576.

32) CCFR limits: Volume 52, Number 16, Physical Review Letters, 16 April 1984.

33) CDHS upper limit : H.J. Meyer et al., Procedings of the European Physical Society HEP 83, Brigton; England (1983)

34) F. Reines et al., Phys. Rev. Lett. 45, 1307(1980).

37) Preliminary results from CDHS on θ_W seem high: C. Gewniger, talk at the EPS HEP Conference, Brighton, 1983.

38) Lepton Mixing and Neutrino Oscillations, S.M. Bilenky and B. Pontecorvo Physics Reports (Section C of Physics Letters)41, No. 4(1978)225-261 North Holland Publishing Company.

39) Decay correlations of heavy leptons:Yung-Su Tsai, Physical Review D, Volume 4, Number 9, 1 nov 1971.

40) B.R. measurement of $\tau \rightarrow \pi^- + \nu_\tau$ and $\tau \rightarrow e^- + \overline{\nu}_e + \nu_\tau$ Volume 109 B, number 1,2, Physics Letters, 11 feb 1982,119.

41) F production: CLEO, A. CHEN et al., Phys Rev. Lett. 51, 634(1983).

42) For a review of θ_W: C. Llewellyn Smith and J. Wheater, Phys. Lett. 105B, 486(1981)

43) Prompt neutrino flux from 400 GeV protons using BEBC, Physics Letters, Volume 96B, number 3,4, 3 november 1980.

44) Weak Inelastic Production and Leptonic Decays of Heavy Leptons, A. Sony, Physical Review D, volume 9, Number 7,1 april 1974(2092).

45) L. Stutte, Proceedings of the 1981 International Conference on Neutrino Physics and Astrophysics, Vol. 1,p. 337, 1981.

46) Beam Simulation: D. Edwards, S. Mori, S. Pruss, Fermilab TM-661, 1976.

47) F.E. Taylor, Procedings of the XVIIth Recontre de Moriond 1982 Vol. 1, p. 267, edited by J. Thanh Van, Editions Frontieres, Gif Sur Yvette,

France.